9-2007

The Effects of Signal and Image Compression of SAR Data on Change Detection Algorithms

Kiran Shenoy

THE EFFECTS OF SIGNAL AND IMAGE COMPRESSION OF SAR DATA ON CHANGE DETECTION ALGORITHMS

THESIS

Kiran Shenoy, 1st Lieutenant, USAF

AFIT/GSS/ENG/07-02

DEPARTMENT OF THE AIR FORCE
AIR UNIVERSITY

AIR FORCE INSTITUTE OF TECHNOLOGY

Wright-Patterson Air Force Base, Ohio

The views expressed in this thesis are those of the author and do not reflect the official policy or position of the United States Air Force, Department of Defense, or the United States Government.

AFIT/GSS/ENG/07-02

THE EFFECTS OF SIGNAL AND IMAGE COMPRESSION OF SAR DATA ON CHANGE DETECTION ALGORITHMS

THESIS

Presented to the Faculty

Department of Electrical and Computer Engineering

Graduate School of Engineering and Management

Air Force Institute of Technology

Air University

Air Education and Training Command

In Partial Fulfillment of the Requirements for the

Degree of Master of Science in Electrical Engineering

Kiran Shenoy, B.S.

1st Lieutenant, USAF

September 2007

AFIT/GSS/ENG/07-02

THE EFFECTS OF SIGNAL AND IMAGE COMPRESSION OF SAR DATA ON CHANGE DETECTION ALGORITHMS

Kiran Shenoy, B.S.

1st Lieutenant, USAF

Approved:

/signed/	17 Aug 2007
Dr. Richard K. Martin (Chairman)	date
/signed/	17 Aug 2007
Dr. Matthew C. Fickus (Member)	date
/signed/	17 Aug 2007
Dr. Howard E. Evans II (Member)	date

AFIT/GSS/ENG/07-02

Abstract

Synthetic Aperture Radar (SAR) is a form of radar that uses post-processed data to simulate a larger aperture antenna and create a more focused, narrower beam. Each pulse is echoed off the ground target and has its amplitude and phase recorded. This processed data, known as phase history, can be used for a variety of applications. It has become a very popular tool due to its ability to be collected from very far distances in adverse weather conditions. Phase history can be used for terrain mapping, remote sensing and automatic target recognition. On an average run, AFRL's experimental test platform collects 1.7 terabytes for a 20 km ground scene. On an average day the platform collects over 272 terabytes.

With massive amounts of data being collected, the need for effective compression techniques is growing. One of the most popular applications for remote sensing is change detection, which compares two geo-registered images for changes in the scene. While lossless compression is needed for signal compression, the same is not often required for image compression. In almost every case the compression ratios are much higher in lossy compression making them more appealing when bandwidth and storage becomes an issue. This research analyzes different types of compression techniques that are adapted for SAR imagery, and tests these techniques with three different change detection algorithms. Many algorithms exist that allow large compression ratios, however, the usefulness of the data is always the final concern. It is necessary to identify compression methods that will not degrade the performance of change detection analysis.

Acknowledgements

To my family, whose greatness I can only hope to aspire to. To "my better half", for putting up with all the times I said I was too busy. A special thanks to Dr. Martin, my advisor, for always being available to answer questions and helping me start from the ground up with signal processing. Additional thanks to Dr. Fickus and Dr. Evans, my other board members, who have helped through their teachings to develop my understanding of MASINT technology and image processing. Finally, I would like to thank my sponsors, Dr. Michael Minardi and Uttam Majumder at AFRL/SNAS.

Kiran Shenoy

Table of Contents

Page

List of Figures

List of Tables

List of Abbreviations

THE EFFECTS OF SIGNAL AND IMAGE COMPRESSION OF SAR DATA ON CHANGE DETECTION ALGORITHMS

I. Introduction

1.1 Problem Statement

Synthetic Aperture Radar (SAR) is a valuable tool used both in the operational field for remote sensing, as well as in the research field for experimental applications such as oil slick monitoring and terrain mapping. Over the past decade, researchers from various government based entities have been studying compression techniques to decrease the size of the data due to its sheer volume. This problem is due to not only storage of the information, but also the amount of bandwidth required to transfer this information from an airborne or space based asset to a ground station. For the most part, research has been conducted on lossless compression which maintains the integrity of the data when it is uncompressed [7, 22, 25]. Lossy compression is usually ignored because the phase history becomes unusable for processing if part of the data is compromised. With the rapid advances in computer processing technology, there has been a movement towards processing information onboard the collection platform and disseminating to the ground station soon after. In the case that images were created with phase history data on board the platform, lossy compression can become a viable alternative. The Air Force Research Labs (AFRL) has looked into the effects that compression of SAR images has had on human analysts with varying results [20]. While some missions do require human analysts, a recent innovation in the Measurement and Signal Intelligence (MASINT) community that does not is known as change detection, which displays changes in the same area over variable time intervals. Effectively this technology could one day allow the system to decide if certain images are worth looking at for analysts. The intent of this research is to

analyze the effects of lossy compression on the ability to perform change detection analysis. Lossy compression is more appealing due to the higher compression ratios it can achieve when compared to lossless compression. Compressed data that can still be used for change detection could reduce the bandwidth required by collection systems dramatically. Scenes where there is no change detected could be filtered out of the transmission queue and drastically improve the efficiency of the warfighter.

1.2 Goals

The goals of this research effort are:

1. To create threshold based change detection algorithms to adjust for various environment types.
2. To create compression algorithms based on Singular Value Decomposition (SVD), Joint Photographic Experts Group (JPEG) and Wavelet Transform standards and adapt them for 8 bit real data, 16 bit complex data as well as the statistical properties of SAR data.
3. Analyze and compare the compressed detection data against the original data sets to find a suitable scheme that will decrease the bandwidth required for transmission, but maintain the integrity of the change mask.

1.3 Scope

This research is limited to investigating the effects of compression on change detection code based on statistical Gaussian correlation, likelihood ratio tests and simple differencing coding. While compression using Wavelet transforms is extensive this study is restricted to three thresholds of both Bi-orthogonal and Daubechie's wavelets. In addition four thresholds of hybrid SVD and a JPEG method adapted with a Fast Fourier Transform (FFT) are examined. All data used in the study is based off a synthetic phase history and includes predominantly forest and desert

environmental scenes. Unfortunately no urban environmental data was available for analysis.

1.4 Overview

This thesis is organized into five chapters. Chapter II, the Background and Literature Review, provides a thorough history of the development of SAR, change detection, and both lossy and lossless compression methods. In addition several papers and recent articles are discussed that show not only the work that has been done in the past, but also the motivations for this research and the selections of each of the compression and change detection algorithms. Chapter III outlines methodology followed for each one of the compression algorithms. Detail as to how each one is designed for SAR imagery is covered. Chapter IV details all of the results of the simulations as well as observations and explanations for the outcomes for each method. The results will not only be broken down by compression method, but also by environment as past studies have shown that in SAR imagery, environment can have an impact on compression and any analysis of compressed data [7]. Chapter V provides the final conclusions of the research as well as recommendations for the future work in SAR compression for specific applications.

II. Background and Literature Review

2.1 Synthetic Aperture Radar

Synthetic Aperture Radar is a increasingly popular remote sensing technology in the MASINT community that fabricates a larger aperture antenna by taking advantage of a moving platform to create higher spatial resolution images. Compared to regular aperture radar, SAR artificially increases the aperture using the same pulse compression technique as used for range detection, which directly increases the azimuth resolution. Returned signals from the ground are processed to form the phase history data which in turn are used to create SAR images. Images are formed by taking a two dimensional Fourier transform of the phase history data. SAR data can be represented as:

$$D(t,\vec{x}) = \iint e^{iw(t-2|\vec{x}-\vec{z}|/c)} A(\vec{z},\vec{x},\omega)\ d\omega\ V(\vec{z})\ d\vec{z} \tag{2.1}$$

where $\vec{x}$ is the vector of flight, $\vec{z}$ is the projected path on the ground, c is the speed of light, A is the amplitude of the signal, t is time and V represents the ground reflectivity function [3]. Each pixel in a SAR image is the magnitude or amplitude of the resulting transform, which suggests that brighter pixels are the result of stronger frequencies in the phase history data.

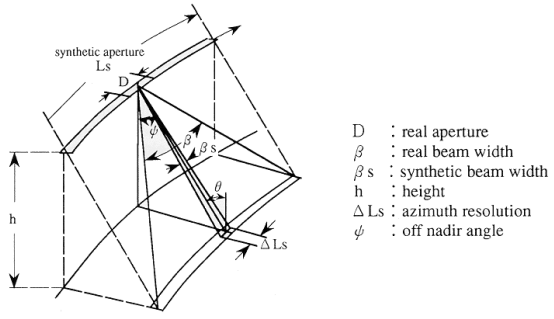

Figure 2.1: Synthesis of a synthetic aperture. As the real aperture D moves across the plane the post processing of the data allows the beam width to expand from β to β_s [30].

2.2 SAR Statistical Characteristics

There are three main statistical properties of SAR that will be exploited in this research effort:

1. The temporal correlation of SAR phase history
2. The semi-redundant nature of SAR data
3. Each SAR image is based on the magnitude of the complex phase history

The semi-redundant nature of SAR phase history is due to the fact that plane waves coming from the ground and hitting the aperture at different times are created from pings from the same field area. This means that for the most part, the same frequencies that occur in one area of the phase history will also occur in other sections of the phase history.

In 2005 Witzgall and Goldstein [29] named this phenomena the "holographic property" stating that "this property [holographic] comes about from the fact that returning plane waves striking the synthetic aperture are generated from the same set of scatters in the field. It implies that phase history statistics are largely stationary." This indicates that since the phase history is stationary, it could be represented with one statistical model for each transformed row of data. Unlike regular images the correlation is not by nearest neighboring pixel but in one dimensional row vectors, which allows the modeling of each SAR image with several one dimensional linear predictors. Another characteristic that can be exploited due to this property is that entropy of each section is low. The repetition of the data allows the removal of redundant phase history in the compression phase. This allows a small fraction of the data to represent the whole. Once the image is formed the phase information is no longer required, which allows for the discarding of the complex data. All three of these properties will be used to tailor three standard compression techniques towards a better SAR compression algorithm.

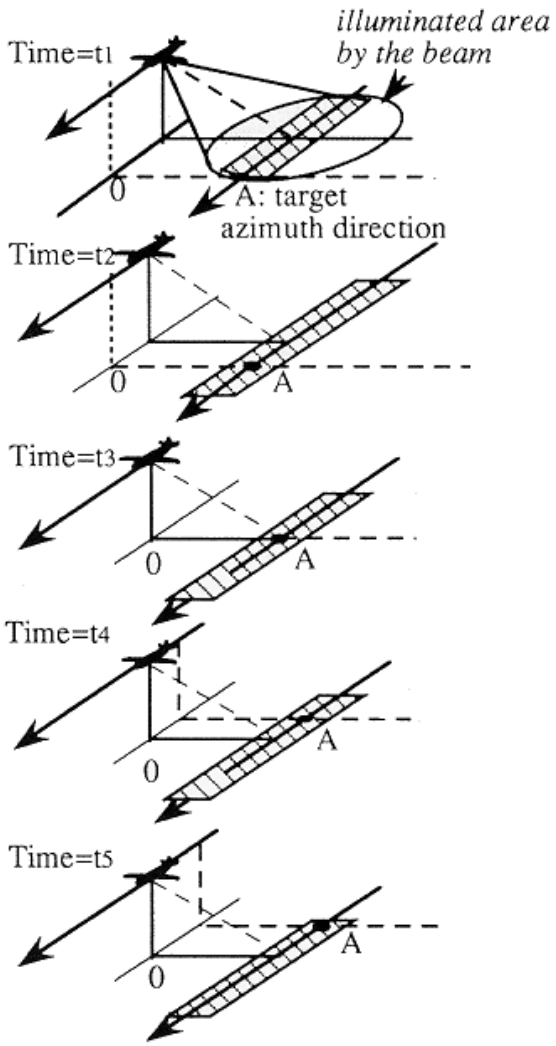

Figure 2.2: Semi-redundant property of SAR. As the collection platform moves forward from time t1 to time t5, point A is still sending return scatter to the platform [30].

2.3 Change Detection

For a compression research effort to be effective, a suitable benchmark has to be selected. While SAR is a valuable tool, its usefulness is only as great as the applications it is used with. One of the most invaluable applications used today in conjunction with SAR is change detection. There are two types of change detection, incoherent change detection, which identifies change in the average backscatter intensity, and coherent change detection which detects change in both the backscatter

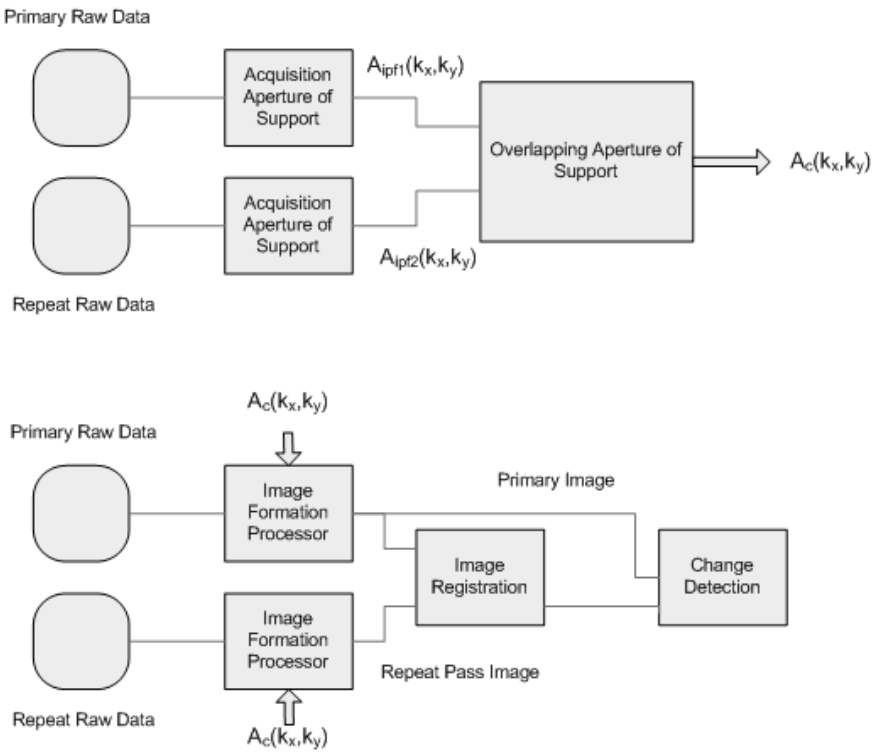

Figure 2.3: Series of steps required in the processing of two SAR images undergoing change detection analysis [17].

intensity and the phase of the complex data. While coherent change detection has the ability to detect very subtle changes, this study focuses on incoherent change detection (hereafter simply change detection) since all the data used in the study is synthetic and has no subtle sub-pixel changes. All compression techniques that are adapted for this study are capable of both and can maintain the phase data if necessary. The defaults for all the algorithms are set to keep only the amplitude of the data while discarding the phase.

Change detection is employed for several applications such as troop movement, heavy armor mobilization as well as the construction of Surface to Air Missile (SAM), sites as seen in many of the SAR images used in this study. While there are many applications of change detection, the basic algorithms used behind the technique are very similar at their core. Since some of these algorithms work better than others in various situations, three different types were selected from many to examine each

scenario. Change in each one of the sets of images is represented in the form of a binary change mask.

$$C(\boldsymbol{x}) = \begin{cases} 1 & \text{if change detected at pixel } x \\ 0 & \text{otherwise} \end{cases}$$

The mask can be created from a number of factors such as movement of objects, the arrival or departure of new objects, and the changing of an object's overall shape.

2.3.1 Geometric and Intensity Tuning. When a collection platform flies at different altitudes, or does not follow the exact same track on the second or any other sequential pass, there are several variations in the imagery that are not true changes in the scene. In order to account for these inconsistencies, geometric and intensity adjustments must be made [18].

The most common remedy to geometric differences, which occurs usually when a platform is collecting at different altitudes or look angles, is image registration, which correctly aligns a series of images into the same globally positioned coordinates. When registering images, a suitable spatial transformation must be selected in order to prevent errors in registration that can create misleading change detection masks. Research has shown that in order to have a good change detection mask produced with less than ten percent error, algorithms must produce a one-fifth pixel registration accuracy [4].

In SAR imagery the magnitude of the intensity of each pixel can vary for the same scene. The majority of the factors for this are due to look angle and altitude. False positives can occur in change detection if the difference in intensity is too great, so adjustments must be made to account for these errors. These include:

1. Intensity Normalization - the pixel intensities of each image have the same mean and variance

2. Homographic Filtering - models each pixel intensity as the product of two components; light source intensity and reflectance. With the aid of a high pass filter, the reflectance part of the intensity can be used in the binary decision step for the change detection mask.
3. Illumination Modeling - using the Lambertian Assumption [19] to account for the difference in intensity between two images.
4. Linear Transformations of Intensity - the use of eigenvectors to transform an image into a different amplitude space before performing the change detection analysis.

In the case of SAR imagery, intensity normalization produced some of the best results for the data used in this research and will be the only intensity adjustments used in this study.

2.3.2 Simple Differencing. Once intensities of the backscatter for all images in a change detection set have been normalized, the easiest way to detect change is to take the difference between the base image, $B(\boldsymbol{x})$ and the image in which we want to see if any change is detected in, $A(\boldsymbol{x})$ [21].

$$D(\boldsymbol{x}) = A(\boldsymbol{x}) - B(\boldsymbol{x}) \tag{2.2}$$

Once the difference has been calculated, change would be determined according to a pre-set threshold τ:

$$C(\boldsymbol{x}) = \begin{cases} 1 & |D(\boldsymbol{x})| > \tau \\ 0 & |D(\boldsymbol{x})| < \tau \end{cases}$$

Using this algorithm, the threshold is selected empirically, so it will rarely outperform other algorithms. In addition, this type of change detection is susceptible to false alarms due to noise and other variations in SAR imagery such as speckle, motion blurring and corner reflectors.

2.3.3 Statistical Gaussian Hypothesis Testing. In the case of a statistical change detection algorithm, a probability is based on two hypotheses. The null hypothesis H_0 in which no change has occurred and the "else condition," and H_1 in which a significant change has happened [11]. H_1 is determined based on the calculation of each joint Probability Density Function (PDF), $p(B(\boldsymbol{x}), A(\boldsymbol{x})|H_0)$ and $p(B(\boldsymbol{x}), A(\boldsymbol{x})|H_1)$. Often change occurs over several pixels so better results are achieved when the change detection decision is based over a block of pixels instead of each individual one. To construct the binary change mask:

$$C(\boldsymbol{x}) = \begin{cases} p(F(\boldsymbol{x})|H_0) < \tau & H_1 \text{ event has occurred} \\ p(F(\boldsymbol{x})|H_0) > \tau & H_0 \text{ event has occurred} \end{cases}$$

where $F(\boldsymbol{x})$ is a Gaussian random variable with zero mean and σ^2 variance. While σ^2 is not known in the beginning it can easily be found by calculating the same PDF on an area of the image that is known to be unchanged. Using the $F(\boldsymbol{x})$ random variable:

$$p(F(\boldsymbol{x})|H_0) = \frac{1}{\sqrt{2\pi\sigma^2}} e^{-\frac{F^2(\boldsymbol{x})}{2\sigma_0^2}} \tag{2.3}$$

This algorithm yields similar results when the Gaussian random variable is replaced a Laplacian random variable [1].

2.3.4 Likelihood Ratio Test. Since the significant change hypothesis, H_1, varies when different image sets are analyzed and are not known *a priori* it is difficult to model the data via parametric distributions. Similarly to the Gaussian model, if both conditional PDFs can be calculated, a likelihood ratio can be determined:

$$R(\boldsymbol{x}) = \frac{p(D(\boldsymbol{x})|H_1)}{p(D(\boldsymbol{x})|H_0)} \tag{2.4}$$

and a threshold, τ determined to be:

$$\tau = \frac{P(H_0)(F_p - F_n)}{P(H_1)(F_n - F_p)} \tag{2.5}$$

where F_p and F_n are the cost of a false positive and a false negative respectively, and $P(H_i)$ is the *a priori* probability that is determined empirically. From a Bayesian perspective, this algorithm minimizes the error of both false positives and false negatives and given the original two images, maximizes the *a posteriori* probability [18]. Similar to the statistical Gaussian methods, this technique works best if analyzed in pixel blocks of empirically determined size instead of a pixel to pixel basis.

2.4 Compression

With 272 terabytes being collected each day on AFRL's experimental platform, storage and bandwidth for transmission of data soon becomes an issue. The need for a way to compress the imagery in such a way that it is easier to store and faster to send while maintaining the ability to perform adequate change detection analysis is crucial. Several researchers have looked at both lossy and lossless compression as ways of compressing SAR imagery. Most lossless compression research acts only on pixel intensity values and disregards the phase component of the data. Since this research bases their techniques on the real part of the complex data, they employ short prediction filters that only take into account the adjacent pixel correlations and therefore can only realize small compression ratios [28]. There are some instances where data cannot be compressed with lossless compression due to the lack of statistical redundancy. For this reason, this study examines the work of lossless compression but focuses the research on lossy compression as a means to drastically reduce the size of the imagery. While certain applications require the entirety of the data to be preserved, change detection can still perform accurate analysis with some data loss.

2.4.1 Compression Theory. Information theory lays stake to much of the theory behind compressing data. The field was pioneered by Claude Shannon in the 1940s and 1950s, but its true potential was only realized decades later. Most compression algorithms rely on the probabilistic nature of the information content of

the data being compressed. Shannon defined information content as:

$$h(x = a_i) = \log_2 \frac{1}{p_i} \tag{2.6}$$

where X is an ensemble of three variables, (x, A_x, P_x). In this series, x represents a random variable, $A_x = \{a_1, a_2, a_3, ..., a_i, ..., a_I\}$ represents all the possible values in the data set and $P_x = \{p_1, p_2, p_3, ..., p_i, ..., p_I\}$ are all the respective probabilities for each value. Equation (2.6) accurately portrays the amount of information content for the event $x = a_i$. From this it is easy to derive entropy, or the average information content of the ensemble:

$$H(X) = \sum_{i=1}^{I} p_i \log_2 \frac{1}{p_i} \tag{2.7}$$

Entropy is considered a vital piece of compression theory because it sets the maximum limit of lossless compression.

With the theoretical bounds set, actual compression methods can be developed and benchmarked against their potential best score. The lossy compression process has three main components: transformation, quantization, and the encoding stages. Transformation breaks down the data into a series of transform coefficients and arranges it in a way to easily spot repetitious data so as to more efficiently code the input stream of data. Quantization takes the transformed coefficients and converts them into a finite number of integer values. Finally the coding stage catalogues each quantization level with its own unique symbol code.

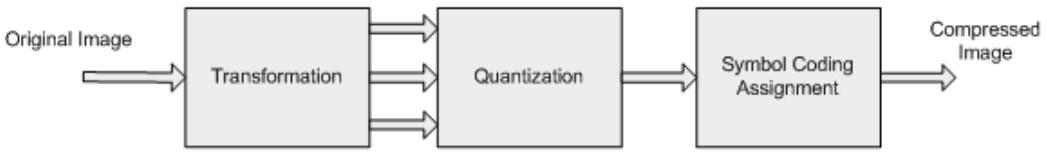

Figure 2.4: Lossy compression components. Each stage represents that of a typical transform coding compression scheme assuming a noiseless channel.

2.4.2 Singular Value Decomposition. SVD is a popular tool in linear algebra for manipulating matrices. In image processing any gray-scale image, or individual layer of a multi-layer image can be viewed as an $m \times n$ matrix. In the case of most color images each layer would be red, green and blue, however, in SAR every pixel is a vector [14]:

$$\vec{X} = \begin{pmatrix} HH \\ HV \\ VV \end{pmatrix}$$

where H is horizontal, V is vertical, and each individual dimension is a complex polarization return.

SVD theory states that if $A \in \mathbf{R}^{m \times n}$ then there exists two orthogonal matrices U and V with orders m and n respectively, as well as a diagonal matrix $\sum$, such that:

$$U^T A V = \sum = \begin{pmatrix} \Sigma_1 & 0 \\ 0 & 0 \end{pmatrix} \tag{2.8}$$

$$A = U \sum V^T \tag{2.9}$$

where $\sum_1$ represents the singular values $\sigma_1 \geq \sigma_2 \geq \sigma_3 \geq \sigma_r \geq 0$ and r is the rank of the original matrix A [23]. While images with high neighboring pixel correlation can have several dependant columns, SAR has very little column dependance and often has rank equal to the amount of columns in the data. Matrices U and V each have one orthonormal basis and are known as the left and right singular vectors respectively. U is $m \times m$, V is $n \times n$, $\sum$ (hereafter known as S) is $m \times n$, and is of the form:

$$A = \begin{pmatrix} \vec{u_1} & \dots & \vec{u_r} & \dots & \vec{u_m} \end{pmatrix} \begin{pmatrix} \sigma_1 & & & & \\ & \ddots & & & \\ & & \sigma_r & & \\ & & & \ddots & \\ & & & & 0 \end{pmatrix} \begin{pmatrix} \vec{v_1^T} \\ \vdots \\ \vec{v_r^T} \\ \vdots \\ \vec{v_n^T} \end{pmatrix} \tag{2.10}$$

With a known A, finding each one of these factorized matrices involves some basic linear algebra:

$$A^T A = (USV^T)^T (USV^T) = VS^T U^T USV^T \tag{2.11}$$

$U^T U = I$ is known since U is an orthogonal matrix which yields the result:

$$A^T A = VS^2 V^T \tag{2.12}$$

By diagonalizing $A^T A$, one can compute the eigenvectors, which are the columns of V, and the eigenvalues, which are squares of the elements of S.

By factoring A into USV^T, compression can be achieving by approximating the original matrix with far fewer matrix entries. Using the rank of the matrix, we can remove all dependant entries which are redundant entries when $r < m$ or $r < n$.

$$A = \sigma_1 u_1 v_1^T + \sigma_2 u_2 v_2^T + ... + \sigma_r u_r v_r^T + 0 \cdot u_{r+1} v_{r+1}^T + ... \tag{2.13}$$

The original image A can be further compressed by dropping off more of the non-zero singular values. Since these values will decrease in order, truncating the coefficients of the linear representation at the end will have less of an effect on the overall image. The effect the number of elements removed will have on the image information is determined experimentally. The more terms we leave off, the better the compression ratio achieved, however, more information is lost as well.

2.4.3 Transforms in Compression. Transforms are valuable tools in image compression because they decrease statistical correlation in an image. In two dimensions, the spatial domain typically has a high amount of redundancy in imagery because neighboring pixels typically share the same amplitude and phase if they all represent one object. A transform allows each of these repeated correlations to be coded only once.

Another added benefit to transforms is their energy compaction property. Energy compaction allows the transform to represent multiple redundant signal energies in a fewer number of transform coefficients. In terms of lossy compression, the probabilistic nature of the coding process would indicate that only the dominant coefficients would represent the image. An individual coefficient in the frequency domain represents one value in the spatial domain. If there exists an image with only one backscatter intensity value, then only one coefficient is needed in the frequency domain. Each of the transform coefficients contain a percentage of the energy of the overall signal, and these fractions represent an energy percentage that has an indirect relationship. In every case, the lower the value of the fraction, the better the energy compaction is [26].

2.4.4 JPEG Compression. The JPEG compression standard describes a general set of guidelines for encoding/decoding techniques, rather than a single algorithm. JPEG was the first international digital compression standard for both color and gray-scale images and was defined in four "operation modes" [9]:

1. sequential Discrete Cosine Transform (DCT) mode - the image is encoded from left to right, top to bottom scan.
2. sequential lossless mode - the image is encoded with no degradation of data but yields a lower compression score.
3. progressive DCT based mode - the image is encoded over several scans where transmission time is not an issue and the image builds become better with each pass.
4. hierarchical mode - the image is encoded at several different resolutions so that lower resolution images may be previewed without having to download larger versions from the beginning.

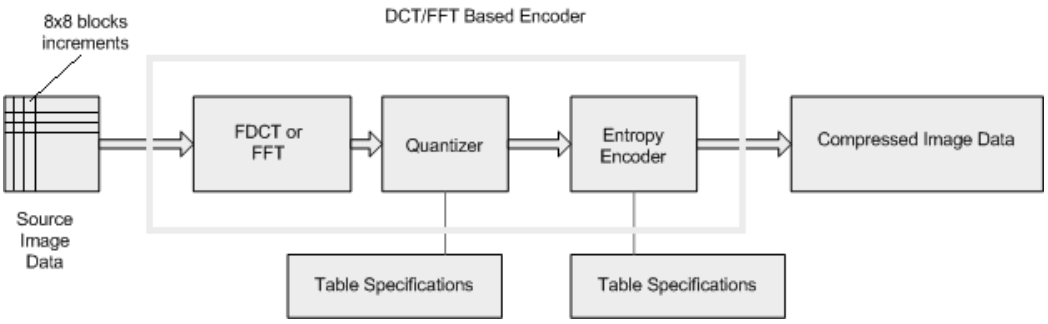

Figure 2.5: Flow chart of the various stages required in JPEG compression [24].

While there are several variations, the method described in this section is the baseline algorithm while modifications and adaptations for SAR imagery will be discussed in Chapter 3.

2.4.4.1 Transformation via the DCT. At the transform phase the input image is broken up into 8×8 blocks which then enter the Forward DCT (FDCT):

$$F(m,n) = \frac{1}{4}C(m)C(n)\Big[\sum_{x=0}^{7}\sum_{y=0}^{7} f(x,y)\cdot cos\frac{(2x+1)m\pi}{16}cos\frac{(2y+1)n\pi}{16}\Big] \qquad (2.14)$$

where:

$$C(m), C(n) = \begin{cases} \frac{1}{\sqrt{2}} & \text{if m,n=0} \\ 1 & \text{else} \end{cases}$$

The JPEG specification allows 8-bit samples per component in DCT operations. Gray scale images only have one component, however SAR and color images have three components that require processing.

2.4.4.2 Quantization. The result of the FDCT is 64 DCT coefficients quantized with a 64 element table. Each table tends to vary by application and usage but is standard in the fact that it is an 8×8 matrix of integer values ranging from 1 to 255. "Coefficients that have zero frequency in both dimensions are known as DC coefficients, while all others are known as AC coefficients." [24] The main purpose of this step is to get rid of any information that won't significantly degrade the image.

In JPEG compression, it is the stage where most of the compression happens and hence where most of the degradation occurs in image quality.

In this step of the compression process, quantization is performed by dividing each individual DCT coefficient by the element in the quantization table with the same indices.

2.4.4.3 Entropy encoding. Once the data has been pre-processed with DC coding and and arranged in the standard zig-zag sequence, the entropy encoder further compresses the image by taking advantage of statistical redundancies. For the coding phase, Huffman coding is used. Huffman coding arranges all available inputs into a table and forms codes by joining the two least probable inputs via addition of their probabilities while tagging each (for this example) with a zero and a one. Each stage of the Huffman coding tree reduces the sample size by one till there are no more left. In the end, codewords are constructed by appending each tag in reverse order until we reach the original value. As the probability of an input increases the length of the codeword decreases. Huffman coding is lossless so the original values before the entropy coding can always be recovered.

2.4.5 Wavelet Transform Based Compression. Wavelet theory has existed since the early 1900s when Haar first discovered a set of wavelets that are now known as Haar functions. However, this science was exclusive to mathematics until only recent times, when it first was applied to signal and image processing. From physics we know that a wave is energy or a disturbance traveling through a medium or vacuum. The easiest examples of this are sound and light respectively. A wavelet is only a piece of wave that is a localized oscillating function. The wavelet transform is given by:

$$f(t) = \sum_{j,k} a_{j,k} 2^{j/2} \Psi(2^j t - k) = \sum_{j,k} a_{j,k} \Psi_{j,k}(t) \tag{2.15}$$

where $a_{j,k}$ are the two dimensional coefficients formed in the transformation process. Similar to the Fourier transform, the wavelet are forms of time-frequency representa-

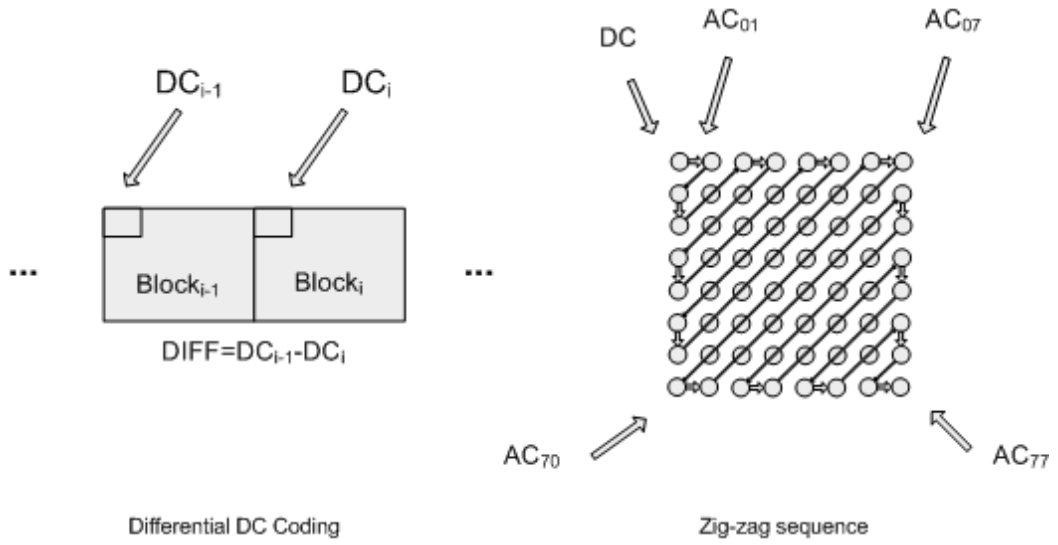

Figure 2.6: To prepare the 8×8 blocks for entropy encoding DC coding in a zig-zag sequence is performed. The quantized DC coefficient of each of the 64 samples is encoded as the difference between the original DC coefficients that are adjacent to each other. The now quantized coefficients are then re-ordered in a zig-zag sequence so that frequency components are encoded from lowest to highest [24].

tion. However, while the Fourier transform is good for modelling stationary signals that have statistical redundancies, wavelets can model non-stationary signals that have no pixel correlations.

There are two main classes of wavelets: time-scale wavelets and time-frequency wavelets. In the case of two dimensions space would substitute for time. All time scale wavelets are derived from a single "mother wavelet" by scaling and translating the original function. Translation occurs over the time axis as the index k changes and scaling occurs as the index j changes. These time-scale wavelets are then used to roughly approximate the original signal or image at a large scale but increase in precision at smaller scales. This is done by splitting the coefficients into detail coefficients and course coefficients via a high pass and low pass filter respectively in the sub-band coding block. In fact one of the main benefits of wavelet compression techniques is the ability for small features in an image to be represented with few coefficients. Economical compression can be achieved by encoding these coefficients.

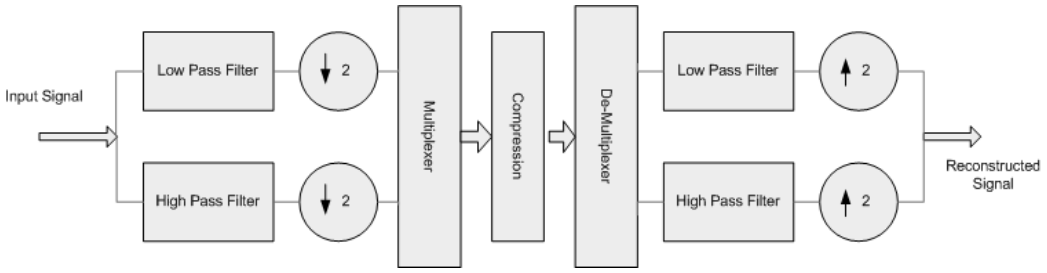

Figure 2.7: The breakdown of a signal into its high and low frequency components. Assuming ideal conditions and no compression is being done in the compression block, the two band technique can output the original signal with zero degradation.

2.4.5.1 Sub-band coding. Sub-band coding splits the original signal into two by filtering both the high and low frequency sub-bands and down-samples each by two. This could be done multiple times splitting the signal into 4,8,... before actually entering the multiplexer as long as there is a corresponding set of up-samplers on the other side of the de-modulator to reconstruct the signal. In the absence of noise and compression, the sub-band coding block can yield a perfect reconstruction. There are, however, conditions that must be met by the high and low pass filters. Given an input, $x_0(n)$ and $x_1(n)$, the linear high pass and low pass filters, $h(n)_n$ and $l(n)_n$, an output signal of the reconstructed signal $(y_n)_n$, such that after a Z-transform, $Y(z) = L(z)X_0(z) + H(z)X_1(z)$ [16] where:

$$X_0(z) = \frac{1}{2}\big[L_1(z)X(z) + L_1(-z)X(-z)\big] \tag{2.16}$$

$$X_1(z) = \frac{1}{2}\big[H_1(z)X(z) + H_1(-z)X(-z)\big] \tag{2.17}$$

substituting the equations:

$$Y(z) = \frac{1}{2}\big[L_2(z)L_1(z) + H_2(z)H_1(z)\big]X(z) + \frac{1}{2}\big[L_2(z)L_1(-z) + H_2(z)H_1(-z)\big]X(-z) \tag{2.18}$$

where $X(z)$ is the original input signal and H_n and L_n are the series of high and low pass filters respectively. According to sampling theory, aliasing can be removed if the

high and low pass filters are defined as [15]:

$$L_2(z) = H_1(-z) \tag{2.19}$$

$$H_2(z) = L_1(-z) \tag{2.20}$$

where perfect reconstruction can occur with the following conditions:

$$\Delta(z) = Q(z) - Q(-z) = 2z^{-m} \tag{2.21}$$

where

$$Q(z) = L_1(z)H_1(-z) \tag{2.22}$$

where $Q(z)$ is known as the product filter and m is the delay due to the system components. While this is the scenario with splitting the signal into two separate high and low frequency sub-bands, a sub-band coding block with more filters changes the conditions [10].

2.4.5.2 Thresholding and Entropy Encoding. Between the modulation and de-modulation compression occurs on the two-dimensional signal. Similarly to SVD, wavelet transforms have a series of coefficients that can be modified to be in a series of decreasing order. Through a technique called thresholding, which is a form of quantization, several of these coefficients that have a lower weight can be made to be strings of zeros. By setting a tolerance below which all coefficients will be made zero, wavelet coefficients with a low weighting can be removed from signal. Once the threshold has been set, Huffman coding can be implemented to compress the data further. The greater the threshold value, the fewer the data points that enter the entropy encoder. These two steps can drastically increase the compression ratio, however there is no algorithm for finding an optimum threshold. The value must be set empirically.

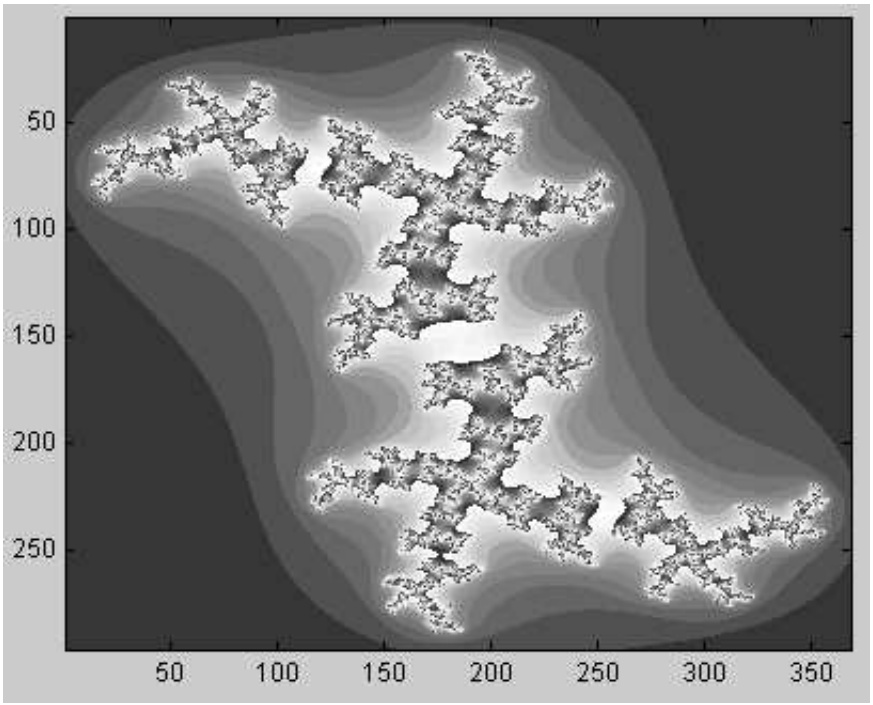

Figure 2.8: The original image before sub-band coding is performed. This is an unprocessed image that is included in the MATLAB® sample library [12].

2.4.5.3 Compression using the Wavelet Transform. While only the Haar wavelet family was pointed out in this section and used in the example of the two level transform, numerous families of wavelets exist and are used in signal and image processing. For the purposes of this research, Bi-orthogonal and Daubechies wavelets will be looked into and developed in Chapter 3.

2.5 SAR Compression Research

Numerous studies have been done on SAR compression methods all having a new technique for compression whether it be lossless or lossy. Most benchmark these algorithms with compression ratios and questionable measure scales for the fidelity of an image [28]. See and Kuperman took several common compression techniques such as multi-resolution encoding JPEG and vector quantization, and benchmarked the compressed data against the originals by using human analysts. While better than random ratings or scales for image quality, the random variable was still tested by a

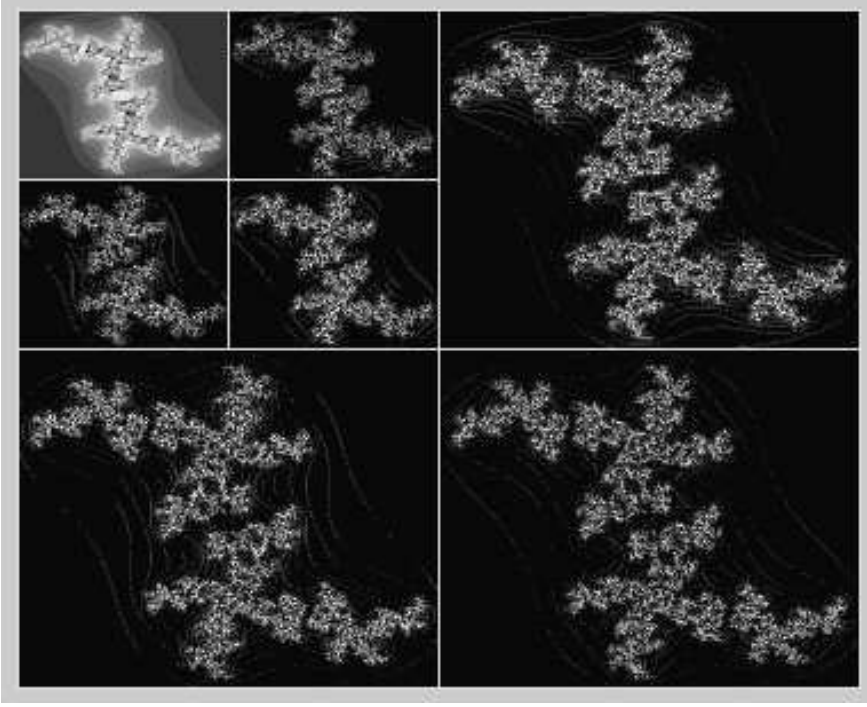

Figure 2.9: The same image after a two level discrete wavelet transform is performed in the sub-band coding stage.

variety of people in which there is still too much variation in the results [20]. While there is no need for scales of quality or problems of reliability in lossless compression, the compression ratios are not high enough for today's needs. In 1999 Ives used multiple-pass gradient adaptive lattice filters to achieve lossless compression, but was only able to achieve a maximum compression ratio 2.56:1 with 16 bit data and 2.19:1 with 8 bit data [7]. For the purposes of this research compression ratio is explicitly defined as the ratio of the original size of the image to the compressed image size in terms of bytes. This phenomena of low compression ratios is not isolated to SAR. In 2005 Wang *et al.* were only able to achieve lossless compression ratios of 3.5:1 with hyper-spectral images. [25]. In order to properly gauge the effectiveness of compressed SAR imagery, a non-variable benchmark with actual results must be implemented.

III. Methodology

3.1 Introduction

In this chapter, an experimental method is explicitly laid out that will accomplish the goals of the research. The data for this research is created from a synthetic phase history for the purposes of training personnel in the analysis of SAR images. The entire data set consisted of specific areas that are modeled after the Siberian forests and plains, however, there is no data for urban environments. Each of the areas has a simulated flight path of a circle, so every scene had a full 360 degree view with the phase history recorded and images formed in 30 degree increments. This data collection is done over 13 non-uniform time intervals. From the large collection of images, several are chosen and are compressed with specifically tuned algorithms and analyzed with a series of benchmarks comparing it to the original data's results.

3.2 Preparation of Data

For the purposes of this research, registered imagery is required where significant change occurred. While there are 26 total collection areas labeled A-Z, some scenes have very similar events. In most scenarios, remote SAM sites are being built or mobilization of heavy armored vehicles is taking place. In some of the areas, no significant change appears to happen at all. From the 26 various collection areas, 5 (D,F,Y and two in G) were selected due to the difference in environment as well as the type and magnitude of the change that occurred in order to create multiple degrees of variability for the experiment. In each one of the 5 areas, one look angle was chosen as well as two successive time intervals that were to be compared. This brings the total number of images analyzed in this to 10. With 11 levels of compression as well as the original data, over 120 images were processed and analyzed for this experiment. From the original data it can be noted that the intensity of each image is not the same. Areas that represent the ground have different backscatter levels that are tuned via normalization. The original data is listed by site:

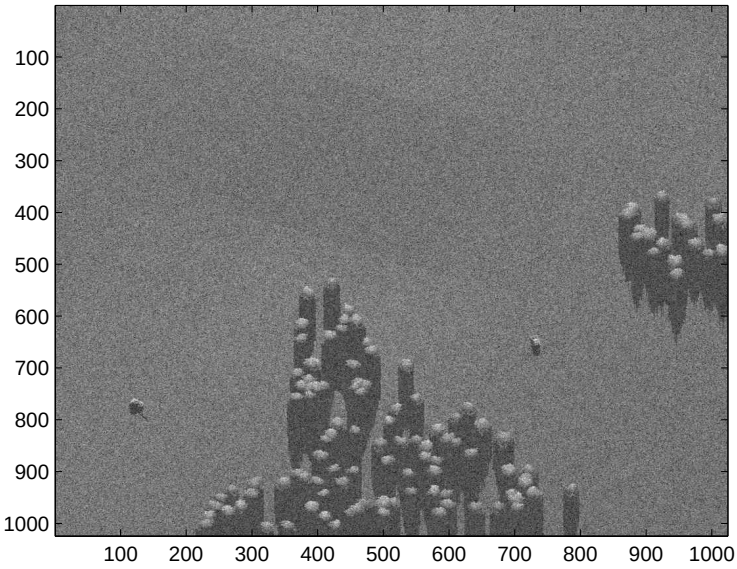

Figure 3.1: Scene D on time interval two.

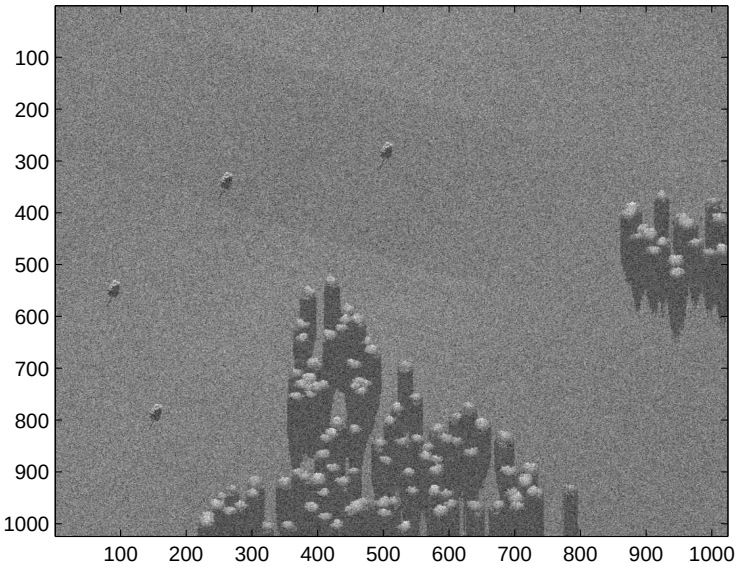

Figure 3.2: Scene D on time interval three.

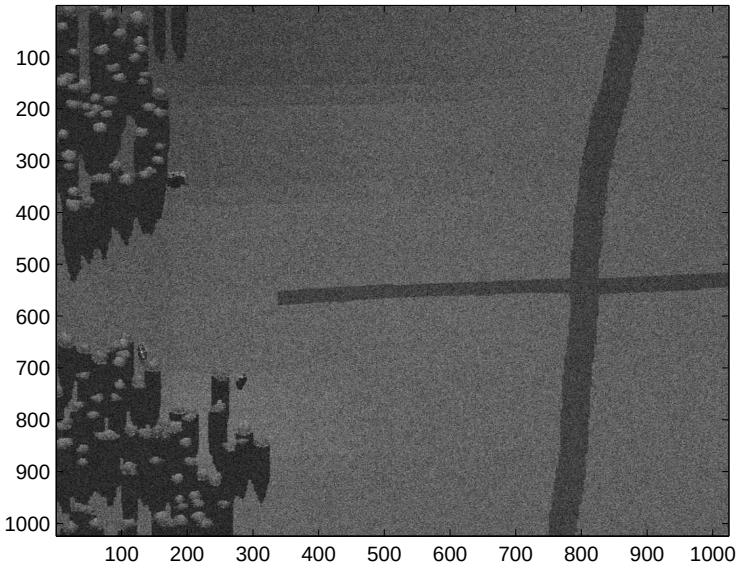

Figure 3.3: Scene F on time interval six.

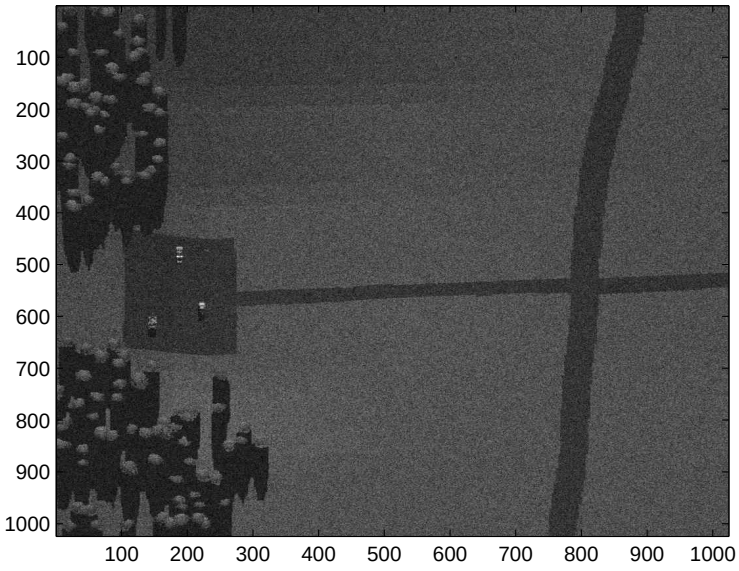

Figure 3.4: Scene F on time interval seven.

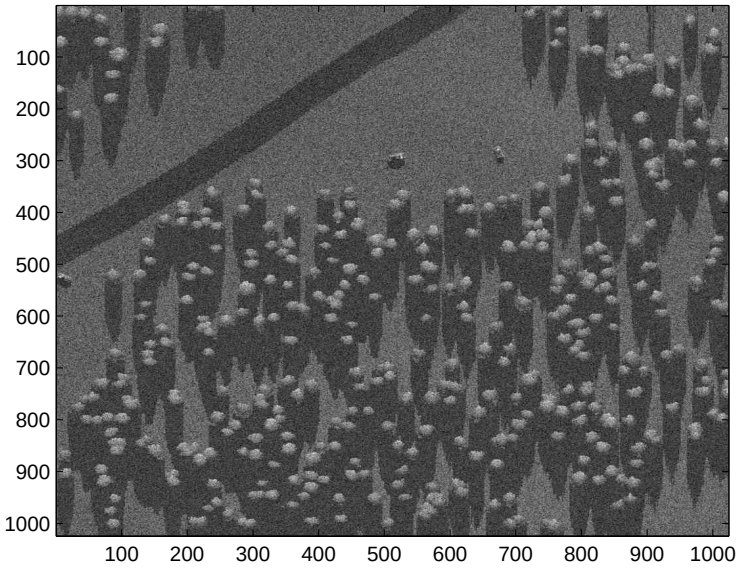

Figure 3.5: Scene G on time interval two.

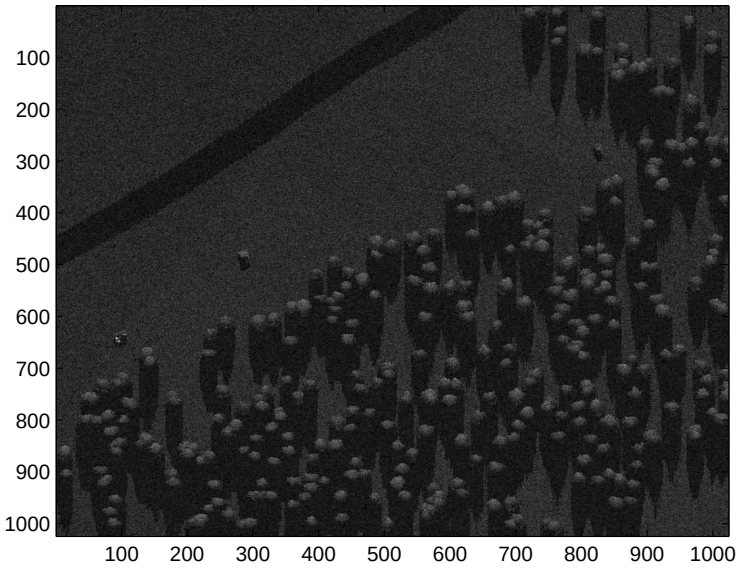

Figure 3.6: Scene G on time interval three.

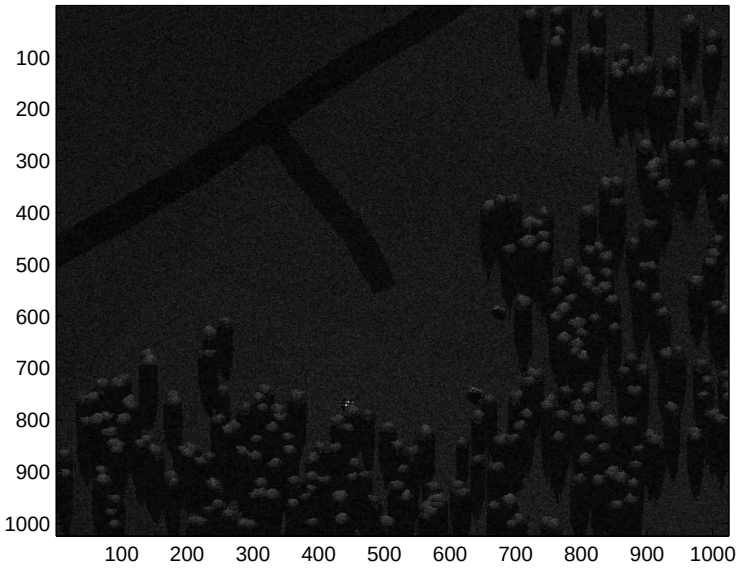

Figure 3.7: Scene G on time interval five.

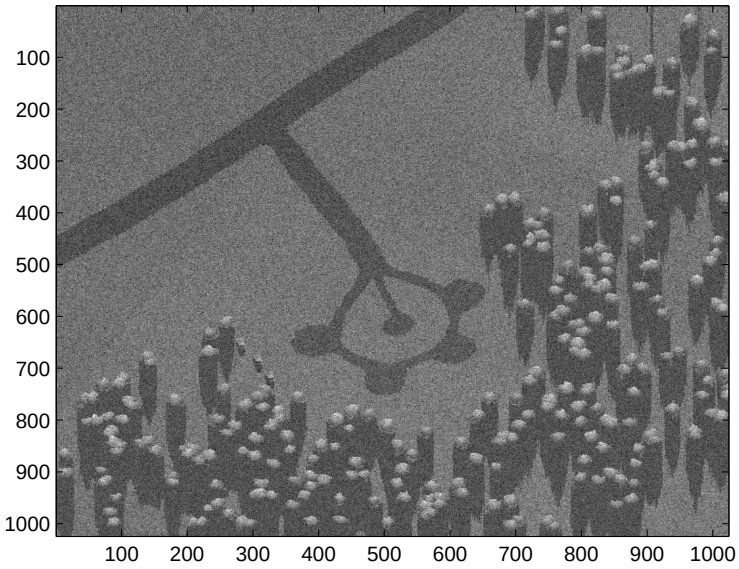

Figure 3.8: Scene G on time interval six.

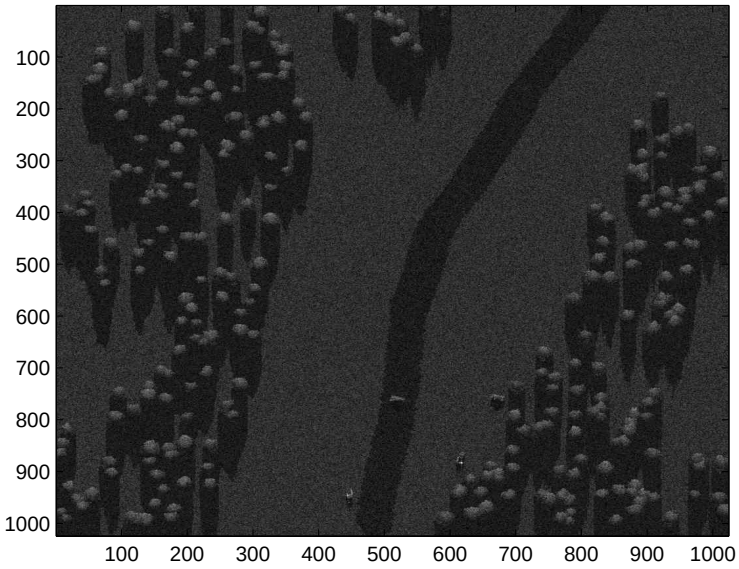

Figure 3.9: Scene Y on time interval twelve.

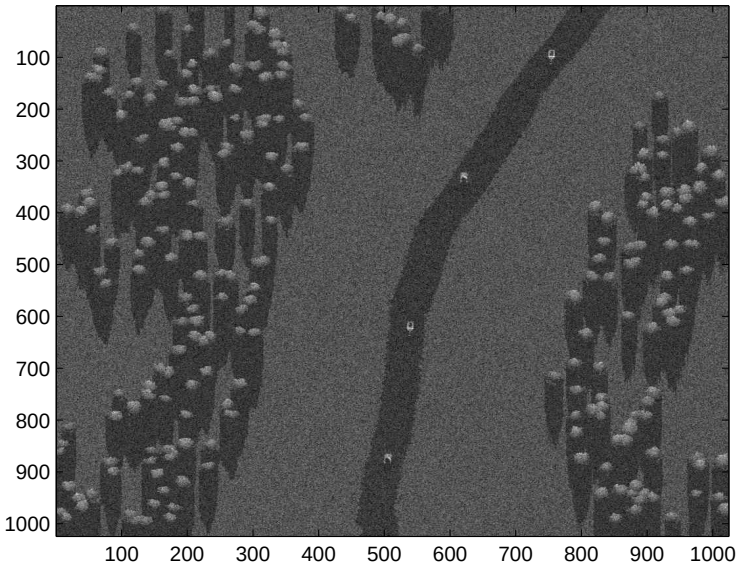

Figure 3.10: Scene Y on time interval thirteen.

Scene D shows the movement of heavy armor across the Siberian plains (Figures 3.1 and 3.2). It has manmade vehicles that move across natural environment. Area F has the building of a large rectangular pavement with vehicles already in place (Figures 3.3 and 3.4). The vehicles offer a closer backscatter value to the original image when compared to the paved section, so this scene was picked to help tune the threshold values of the change detection algorithms. The first set of images from area G, G_2 and G_3, shows movement of construction and demolition vehicles and an area of forrest being cleared (Figures 3.5 and 3.6). This scene has a great amount of entropy with the amount of foliage that is included. The second set of images in G, G_5 and G_6, uncovers a simple SAM deployment site under construction (Figures 3.7 and 3.8). There is a large difference in the backscatter intensity in the two images despite it being the same area. It was chosen to perform intensity tuning to the detection algorithms. The final scene Y, has 4 vehicles moving from the southern portion of the image towards the north along the road (Figures 3.9 and 3.10). The last scene has movement over a man-made surface and change in intensity. The combination of the two made it an ideal candidate for analysis.

3.3 Compression Methods

This section outlines the compression methods used as well as any changes that were made to adapt the algorithm to SAR data. Compression algorithms can be sorted with eight differentiators [20]:

1. Attainable compression ratio
2. Attainable image quality
3. Conformability with SAR data
4. Channel error sensitivity
5. Computational complexity
6. Maturity of algorithm

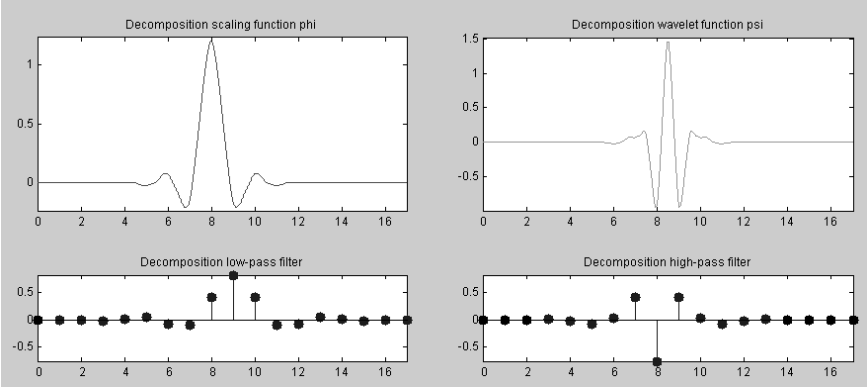

Figure 3.11: The bi-orthogonal 6/8 scaling and wavelet functions for decomposition as well as their high and low pass filters.

7. Inter-operability

8. Progressive transmission capability

Of the eight differentiators, the top three were given the most importance when choosing compression algorithms. While there are countless types of compression models available and still more being researched in the current day, schemes involving the Wavelet Transform (WT) and the DCT have shown promising results with SAR data and will be focused on in this research.

3.3.1 Hybrid SVD. The basic SVD algorithm was first discussed in Section 2.4.2. In this section, modifications to the basic algorithm are detailed. The original $m \times n$ image $B(x, y)$ is transformed via a discrete wavelet transform to deconstruct $B = USV^T$ using the 6/8 bi-orthogonal wavelet family. The image is then decomposed using SVD into the three matrices and is compressed via the Set Partitioning in Hierarchical Trees (SPIHT) algorithm [2].

SPIHT utilizes the redundancy in each of the sub-bands in the wavelet decomposition to prioritize which bits of information content are the most important. Quantization is uniform and is done only after the decomposition of the wavelet is achieved. Each of the wavelet coefficients are ordered by the importance of each piece of data based on a hierarchial tree structure. Since the data is ordered from most

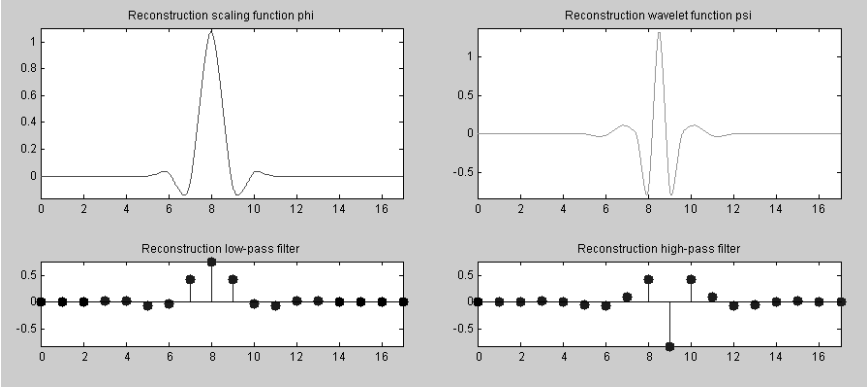

Figure 3.12: The bi-orthogonal 6/8 scaling and wavelet functions for reconstruction as well as their high and low pass filters.

important to least, coefficients can be zeroed from the end to make the data achieve higher compression ratios. In this experiment the first 25, 50, 75 and 100 out of a potential 400 coefficients were retained and processed for each of the data scenes. Each one is then benchmarked and compared using the three change detection algorithms from Section 2.3. This method was chosen due to the fact that it exploited redundancy in the sub-bands from wavelet decomposition rather than neighboring pixel correlation. This technique allows even less symbols to be used in the coding process since neighboring pixel correlation isn't nearly as strong in SAR when compared to standard linear shift invariant images.

3.3.2 JPEG. While the standard method of JPEG compression is used for this research as described in Section 2.4.4, the need for the algorithm to handle both 8-bit and 16-bit data is necessary. To handle this requirement, the FFT is implemented as an option to the standard DCT. The FFT is slightly different in that it uses both sine and cosine waves to model a signal whereas the DCT only uses the latter. While most researchers only use the DCT for image compression because it only has half of the cycle basis functions and is therefore better for smooth transitions in backscatter across several pixels, SAR data doesn't always follow this behavior. Each coefficient, whether transformed via the FFT or DCT, was represented as $F(x, y)$ and

was compressed using:

$$I(x,y) = I_{Round}(\frac{F(x,y)}{Q(x,y)}) \tag{3.1}$$

where the function I_{Round} rounds off the inner value to the nearest integer and $Q(x,y)$ is the quantization table used for all ten images in this study is:

$$Q(x,y) = \begin{pmatrix} 16 & 11 & 10 & 16 & 24 & 40 & 51 & 61 \\ 12 & 12 & 14 & 19 & 26 & 58 & 60 & 55 \\ 14 & 13 & 16 & 24 & 40 & 57 & 69 & 56 \\ 14 & 17 & 22 & 29 & 51 & 87 & 80 & 62 \\ 18 & 22 & 37 & 56 & 68 & 109 & 103 & 77 \\ 24 & 35 & 55 & 64 & 81 & 104 & 113 & 92 \\ 49 & 64 & 78 & 87 & 103 & 121 & 120 & 101 \\ 72 & 92 & 95 & 98 & 112 & 100 & 103 & 99 \end{pmatrix}$$

The element-by-element division of each pixel in the original image with the corresponding quantization matrix element outputs a step size that is normalized. The purpose of this quantization is to represent the DCT or FFT coefficients with as few bits as possible without significantly degrading the image. This section of the JPEG process is where a majority of the compression occurs. Different quantization tables will yield different compression ratios. After all the data is quantized, Huffman coding was used in the encoding processed according to the JPEG specs.

3.3.3 Biorthogonal and Daubechies WT compression. When considering compression using a wavelet transform in this research as described in Section 2.4.5, two mother wavelets were chosen to be compared. The same bi-orthogonal wavelet family was chosen that was used in the Hybrid-SVD compression to compare the differences between the two. In addition, it also was chosen because it is one of the suggested families of wavelets for the new JPEG-2000 file format that is being proposed. The Daubechies 5 wavelet type was also selected because of the differences in the high and low pass filters to give a unique look at what happens in compression

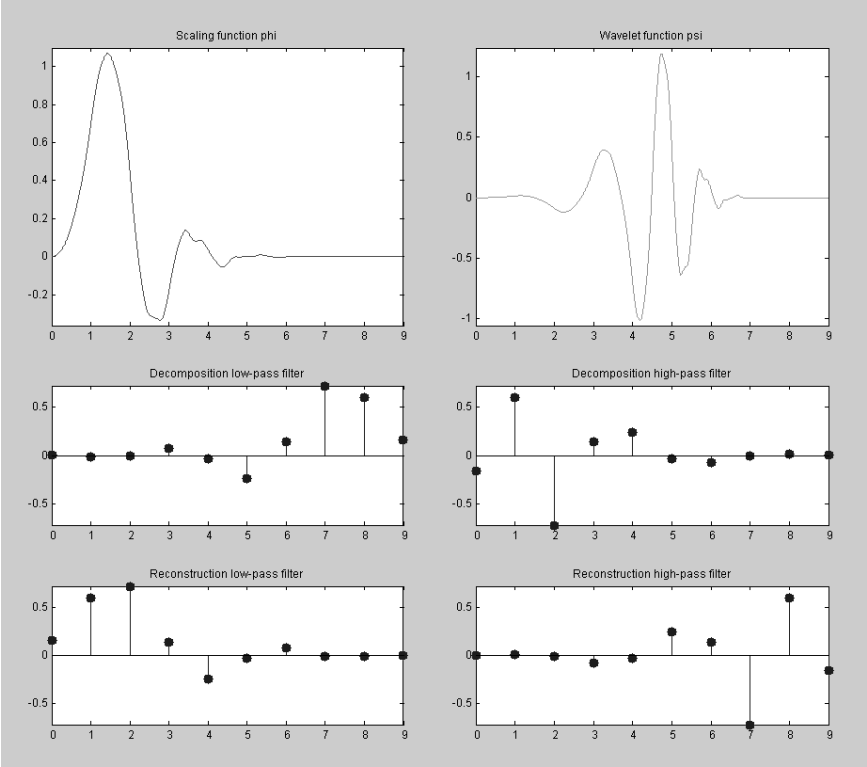

Figure 3.13: Unlike the bi-orthogonal scaling and wavelet functions there is only one for Daubehcie's wavelets. The deconstruction and reconstruction high and low pass filters shown are based on the same set of functions.

and change detection as a result of a change in the filtered signal. Each of the wavelet types were examined using level two decomposition and had their coefficients quantized and then weighted using an adaptive arithmetic coding process [13].

In the adaptive arithmetic coding process, coefficients are separated into several groups that have adaptive probability models based on the decomposition of the original image. Since a majority of wavelet coefficients are close to zero there are several groups that are non-uniform and are focused around this value. Similar to Huffman coding, arithmetic coding can significantly compress data by assigning fewer bits to symbols that are more probable. The probability model for the symbols changes as the data is being processed. Instead of using training data, the weighting is determined based on the data seen thus far in the image. This allows any image to be run through the data without the need for prior knowledge of the images.

For the purposes of this research, block based quantization occurred using the following matrix for all of the wavelet filters:

$$Q(x,y) = \begin{pmatrix} 8 & 7 & 8 & 8 & 34 & 34 & 34 & 34 \\ 7 & 7 & 8 & 8 & 34 & 34 & 34 & 34 \\ 8 & 8 & 12 & 12 & 34 & 34 & 34 & 34 \\ 8 & 8 & 12 & 12 & 34 & 34 & 34 & 34 \\ 34 & 34 & 34 & 34 & 55 & 55 & 55 & 55 \\ 34 & 34 & 34 & 34 & 55 & 55 & 55 & 55 \\ 34 & 34 & 34 & 34 & 55 & 55 & 55 & 55 \\ 34 & 34 & 34 & 34 & 55 & 55 & 55 & 55 \end{pmatrix}$$

This matrix could be scaled to achieve different bit rates, but the ultimate goal was to apply wavelet transform based compression that used many of the standards currently being researched for the JPEG-2000 compression standard. Wavelet transforms had thresholds that can be assigned as described in Section 2.4.5 that allow us to zero out certain coefficients before the quantization process. For each of the wavelet families hard thresholds of 25, 50 and 75 were set in turn. If the value of the wavelet coefficient falls below those values, it would automatically be assigned a zero weighting and not affect the image. The goal is to remove as much information as possible without losing too much detail in the image to perform the change detection analysis. A threshold of 0 yields a perfect reconstruction of the original image if no quantization took place. As the threshold increases, the fidelity and entropy of the image decreases [6]. While thresholds could have gone higher, too much information is lost, resulting in an image that is of no use.

3.4 Change Detection Analysis

Most of the change detection algorithms used in this study are threshold based. Studies have shown that these detection algorithms are environmentally sensitive [8] and can effectively create more false positives and negatives, distorting the results of

the analysis. For this reason multiple change detection algorithms are used. While some of them can obtain their own threshold values through statistical regression analysis of the image, others had to be determined empirically. Since environment can play a factor in creating false hits, for the purposes of this research, scenes with multiple environmental factors such as man made roads, vehicles, natural forest and plains, had two different algorithms working simultaneously with different threshold values. In this experiment the statistical Gaussian method looks for coarse change, such as vehicles and roads, with a lower than normal threshold. At the same time, the likelihood ratio test looks for finer changes, such as natural environmental movements, with a threshold set slightly higher than normal. The union of these two masks will create a single change mask with less error.

While finding a finely tuned change detection method to work with SAR imagery and compressed data is important, it is not the main focus of the research. There are several application specific algorithms in the remote sensing community that outperform the ones that are in use for this research. These algorithms were created to benchmark the compressed data to analyze how reliable the masks created would be for operational requirements. While the threshold values were picked to decrease the amount of error included in the binary change mask, the main goal is to see how much error is induced by the compression algorithm, not the actual change detection itself.

3.5 Relevant Data Retention

With the creation of change detection masks, we not only have a tool that can be used to study what happens in a scene for military operations, we also have all the relevant information for the removal of redundant information from any subsequent images that follow the original. For example, if we look at a pair of images where two vehicles move from one area to another, the change detection mask will label all pixels where actual change has occurred in a scene. There is no need to keep any information from the second image other than what has been detected as significant

change from the first. Therefore, in this research effort, after compression has been completed and change detection analysis performed, file sizes are further reduced by percentages inversely proportional to the amount of change in the scene. For collections of multiple images, each one must be referenced back to the first image, not the one that proceeded it to decrease the amount of bandwidth required. In principle each image could be created from the preceding image, however, this only holds true if permanent change has taken place over the course of each successive image. In order to account for the variability in change, one reference image must be used. For the purposes of this research, this was only done to the backscatter intensity. This, however, could easily be applied to phase history data as well, greatly reducing the amount of data required to be stored and transmitted.

3.6 Conclusion

With all the compression schemes analyzed, the goal of the methodology presented in this chapter is to ultimately have a high probability of detection with a low probability of a false positive. Even with potentially near perfect results, since all the methods used here are lossy compression methods, some information is forsaken for the sake of higher compression ratios. As a result, there will be some error induced in each binary change mask. Unless lossless compression is implemented there is no chance for a perfect reproduction of the original change mask. In the end, while the benchmark serves as a indication as to whether acceptable methods of lossy compression can be implemented, it ultimately depends on the application that the data is going to be used for. This series of experiments is important because it lays the foundation for benchmarks based on an automated computer based decision process rather than human observers. If the results fall within the accepted limits of error for any application it can drastically reduce the amount of man-hours spent on analyzing imagery.

IV. Results

This chapter outlines all the results of the entire research effort. Even though only a small set of data was analyzed, for every two scenes analyzed for change, 34 additional data sets (11 compression levels for each original scene and a total of 12 change detection masks) had to be created to process and analyze the data. Section 4.1 goes through each area selected and gives a baseline change detection mask for which all other data will be compared. Section 4.2 shows the results of each one of the compression methods as well as highlights any qualities that make each compression method better or worse than the others. After compression occurs each one of the compressed scenes are processed with the change detection algorithms and evaluated in Section 4.3. Finally, in Section 4.4, all the data is compared using several analytical tools showing which compression methods were more suitable based on the area examined.

4.1 Original Data Masks

To provide a series of benchmarks, thresholds had to be assigned to the statistical Gaussian method as well as the likelihood ratio hypothesis tests that slightly deviated from the normal threshold value to account for both coarse and fine changes in the scene. For each of the data sets, the original data that would be used as the standard for comparison is shown in Table 4.1. In this table, τ_{SG} and τ_{RT} are the change detection thresholds for the Statistical Gaussian method and the Likelihood Ratio Test respectively. For the purposes of clearly illustrating change and the effects of post compression change detection, pixel blocks of 401×401 were selected and processed in this experiment. The column in Table 4.1 titled "sub-image location" gives the rows and columns of the pixels selected for processing. These are the areas in the image where most of the change has occurred and therefore removes the data that is not of concern. "Elapsed time" is the average processing time over six runs for the 401×401 pixel blocks listed. The CD masks for the five selected scenes are shown in Figures 4.1 to 4.5. The averaging processing time, $\bar{t}$, for an entire 1024×1024 SAR image is 294.13 seconds. This time includes the operation of both algorithms and the

Table 4.1: Reference Data.

Set	Images	τ_{SG}	τ_{RT}	sub-image location	elapsed time
D	2,3	0.511	0.526	400:800,1:401	$45.80s$
F	6,7	0.308	0.312	400:800,1:401	$38.77s$
G_1	2,3	0.101	0.120	1:401,1:401	$43.82s$
G_2	5,6	0.212	0.228	400:800,400:800	$53.22s$
Y	12,13	0.381	0.400	600:1000,1:401	$40.34s$

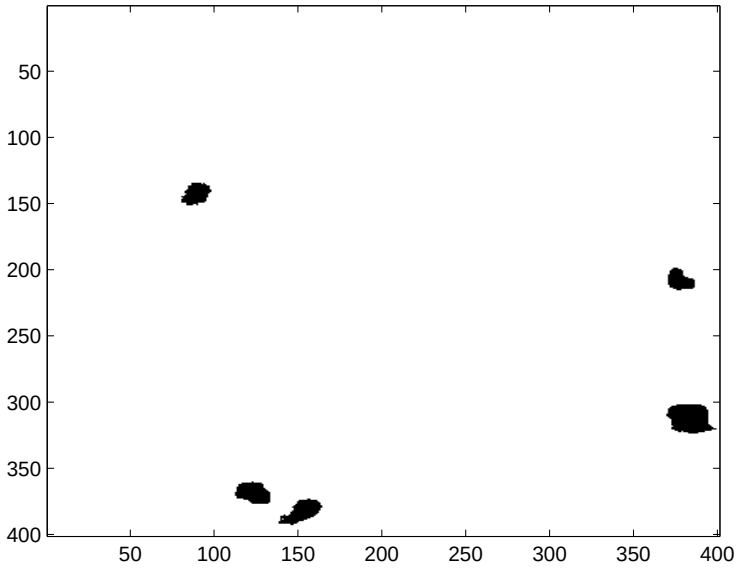

Figure 4.1: The change in mask D is represented by the movement of ground vehicles.

intersection of both masks into one. From analyzing the results of entering different threshold values it is found that elements introduce increased entropy decreased the computed threshold value of the change detection mask. This decreased value causes more false positives to occur and serves to support our hypothesis that two algorithms working at different threshold values are necessary.

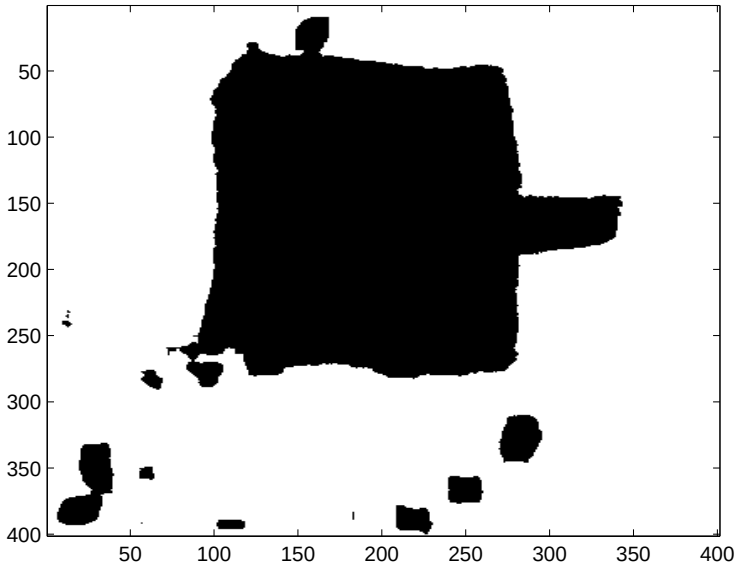

Figure 4.2: Mask F has a movement of vehicles, the creation of a large tarmac area, and the removal of a few trees that obstructed the area.

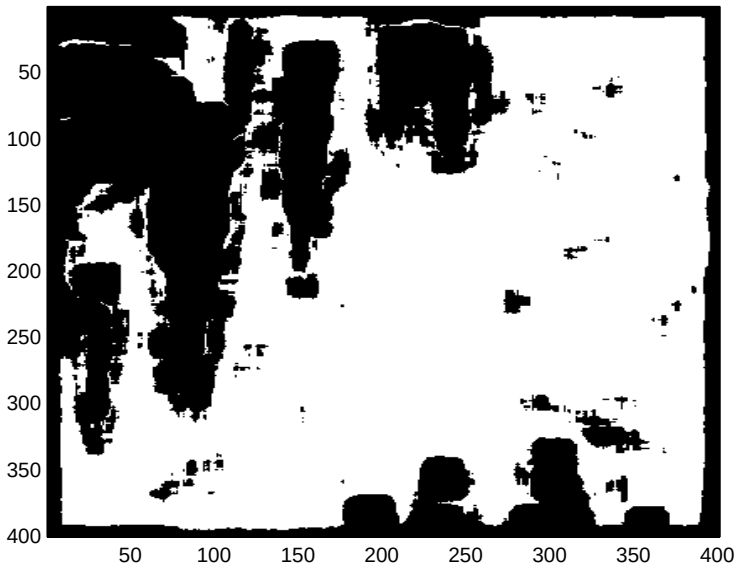

Figure 4.3: The first mask in area G has the greatest entropy of all the images due to the large amount of forest in the scene. Most of the false hits can be attributed to noise in the data as well as simulated movement of foliage. The increased entropy, combined with the zero padding in the CD algorithms, created a border effect showing change around the edges where it shouldn't occur.

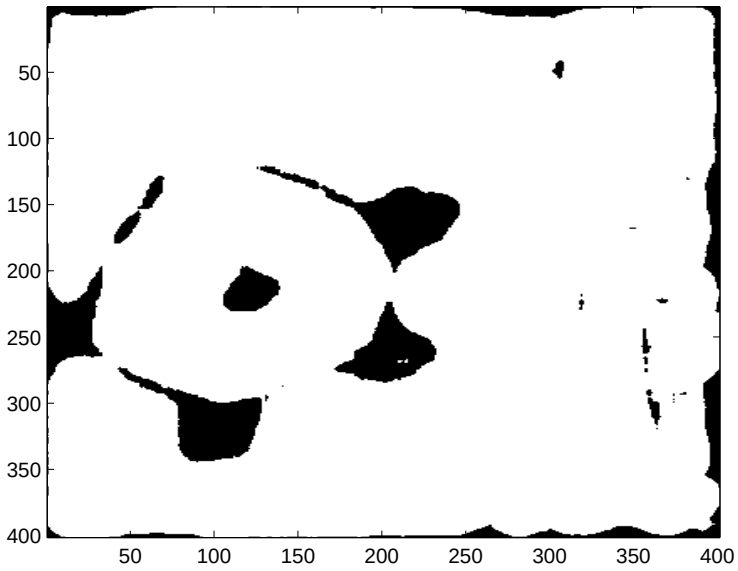

Figure 4.4: The second mask in G has the change registering as the construction of a new SAM site. The small spot in the top right is due to the movement of a vehicle. Here part of the ring created in the second scene doesn't register as change due to errors caused by the intensity tuning of the second image.

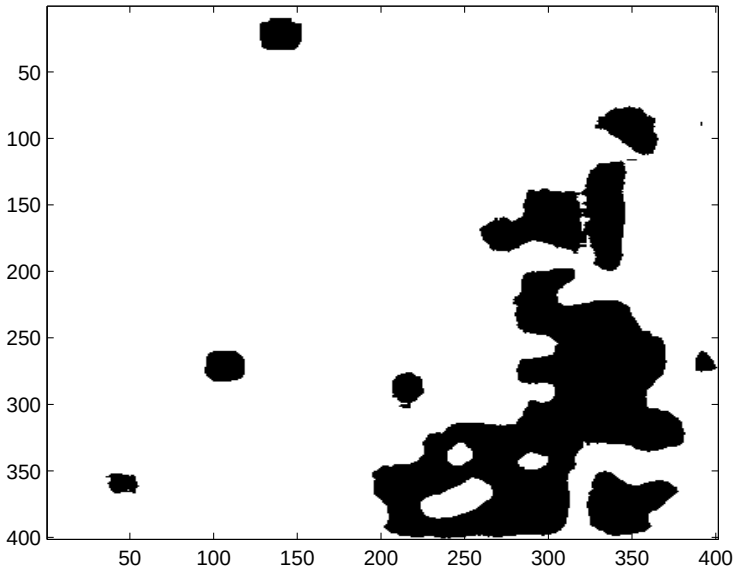

Figure 4.5: The mask produced from the change in Y accurately detected the movement of vehicles along the road as well as a number of trees that were removed from the scene.

While these masks do not show what has originally moved from the first scene and what is no longer in the second for the corresponding pixels and vice versa, this can be easily added via an additional post-processing step. This, however, does not affect this research effort and was therefore not included.

4.2 Compression Results

Due to the number of images processed in this research only one to two scenes per method will be illustrated in this section. For additional data sets please see Appendix A.

4.2.1 Error Metrics. When comparing the algorithms for effectiveness, two additional Measures of Effectiveness (MOE) will be referred to on numerous occasion. The first is Mean Squared Error (MSE), which is the average of the squared difference between the original $M \times N$ image, $O(x, y)$, and the compressed image $C(x, y)$.

$$MSE = \frac{1}{MN} \sum_{x=1}^{M} \sum_{y=1}^{N} \left[O(x, y) - C(x, y) \right]^2 \tag{4.1}$$

The lower the value the better since MSE is essentially summing up the error at every pixel. This has an inverse relationship with the second metric, which is Peak Signal to Noise Ratio (PSNR) which measures the ratio between the signal which in this is $O(x, y)$ and the noise which is the amount of error induced in the original image due compression.

$$PSNR = 20 \log_{10} \left(\frac{255}{\sqrt{MSE}} \right) \tag{4.2}$$

For the purposes of this research, MSE is always unitless and PSNR is measured in decibels (dB).

4.2.2 SVD Analysis. The SVD algorithm when combined with a wavelet transform, yields better results in terms of PSNR and MSE, than SVD alone. The compression ratio was easily changed based on the number of coefficients that were

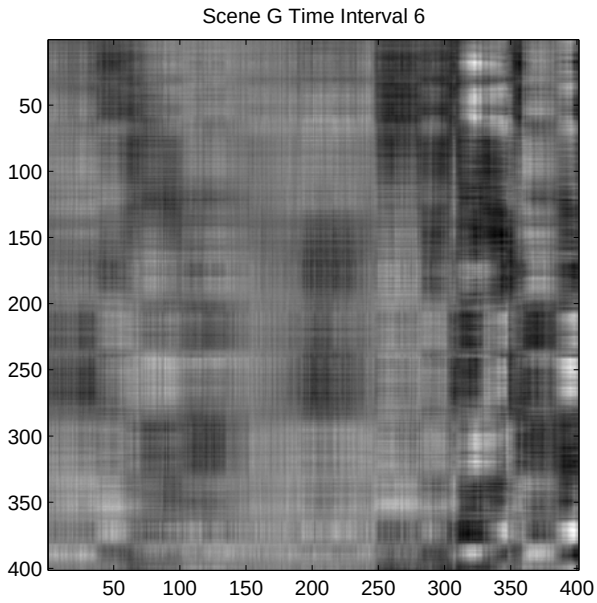

Figure 4.6: Hybrid SVD with 5 coefficients.

assigned a zero weighting. In this study, the first 25, 50, 75 and 100 coefficients were taken into account for the formation of the image to see how drastically the image was affected. The compression ratios ranged from 9:1 with twenty five coefficients all the way to 2:1 with 100 coefficients. As the number of coefficients increased the amount of effect they had on the image decreased exponentially. To illustrate this point additional data points of 5 and 10 coefficients were processed for area G.

As the number of coefficients representing the image went from 75 to 100, there is not much difference visible to the naked eye, however, there are several variations at the pixel level that will be detected with the change detection algorithms. For regular SVD compression the PSNR of the images ranged from 28 dB at a 4:1 compression ratio to 26 dB at 16:1. The Hybrid-SVD method decreased from 39 dB to 34 dB for the same range of compression ratios.

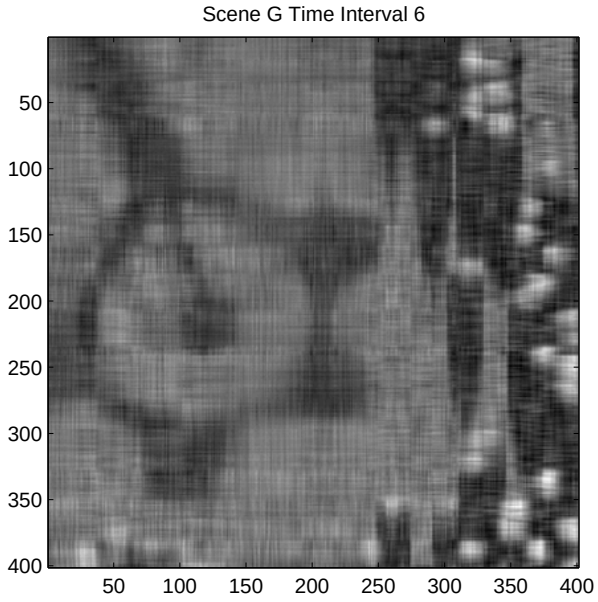

Figure 4.7: Hybrid SVD with 10 coefficients.

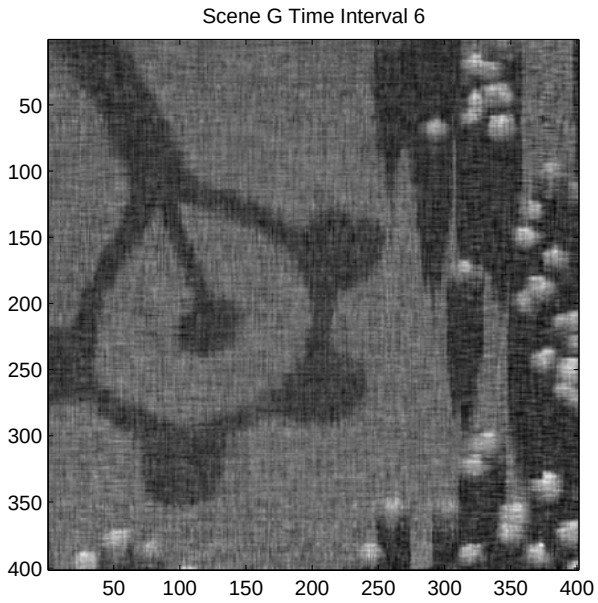

Figure 4.8: Hybrid SVD with 25 coefficients.

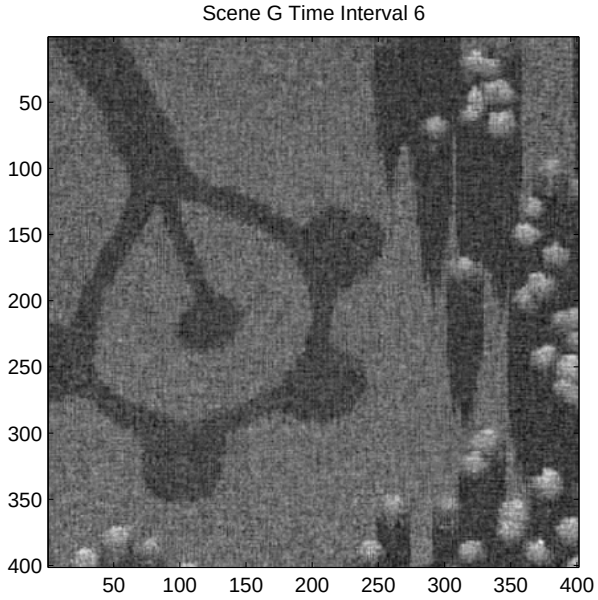

Figure 4.9: Hybrid SVD with 50 coefficients.

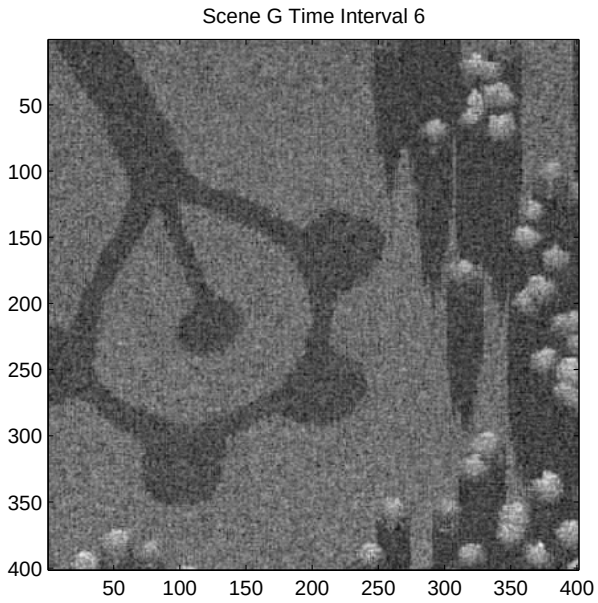

Figure 4.10: Hybrid SVD with 75 coefficients.

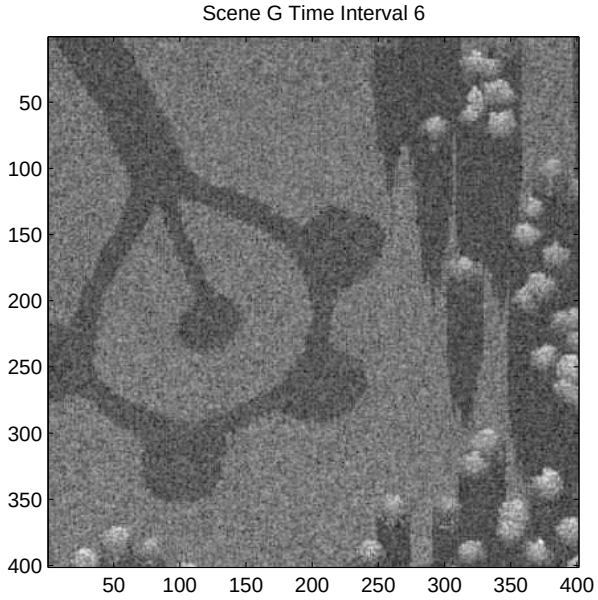

Figure 4.11: Hybrid SVD with 100 coefficients.

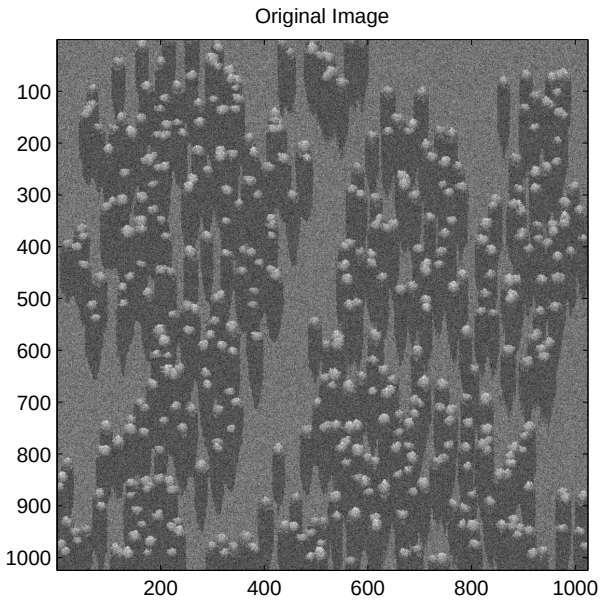

Figure 4.12: The original uncompressed image of scene Y on time interval two.

4.2.3 JPEG Analysis. Of the three compression techniques, JPEG is the only one that is currently included in the National Imagery Transmission Format Standards (NITFS). For general (linear shift invariant) imagery it is an attractive choice due to its low MSE and the resulting high PSNR. For this study, JPEG was analyzed at compression ratios in $2^n : 1$ intervals from $n = 0, 1..., 6$. It was found that due to the JPEG algorithm, specifically the processing of a non-linear shift invariant image with a discrete cosine transform, that objects with intensities that were extremely high or low in the image created a a "padding effect" around them when compressed. This made the compressed images appear to have larger objects when compared to the original image. As an example "SAR shadows" created from the collection platform's line of sight grew by 2-3 pixels in both the x and y directions. This was the predominant effect in the tests with compression ratios greater than or equal to 16:1. While this is the end result of the compression of the given data which is simulated, it can be assumed that this effect will only be magnified in real SAR data when there are additional noise variations that occur. While this phenomenon isn't

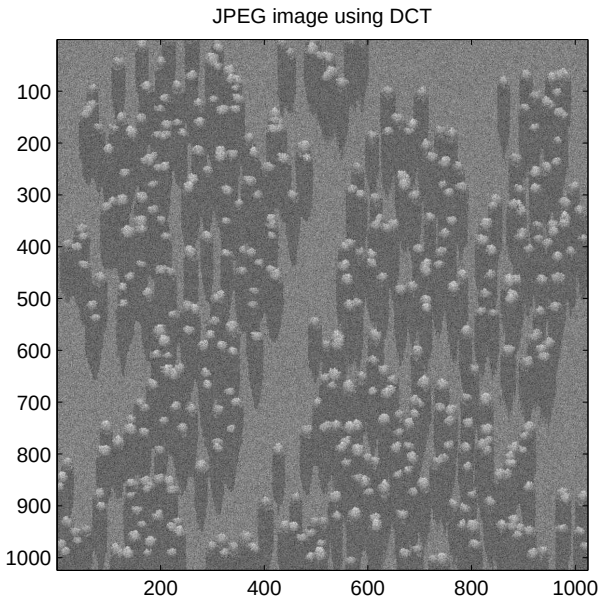

Figure 4.13: The same scene from Figure 4.12 after JPEG compression. This image illustrates how padding doesn't seem readily apparent to the naked eye.

very noticeable to the human eye as seen in Figures 4.12 and 4.13, CD analysis will be altered by this effect due to the extremely high number of false positives that show up on the JPEG image when compared to the original. Over the range of compression ratios 2:1 to 64:1, the PSNR declined the most of all the compression algorithms from 37.5 dB to close to 22 dB.

4.2.4 Wavelet Transforms Analysis. In order to analyze whether different wavelets had a significant impact on the compression and change detection analysis, both Daubechies and Bi-orthogonal wavelets were looked at. Since wavelets are currently being examined for the JPEG-2000 standard, the same de-construction and quantization metrics were used as discussed in Section 3.3.3. The two level decomposition separated each approximation into their horizontal, vertical and diagonal information, which could be perfectly reconstructed if no compression took place after the decomposition.

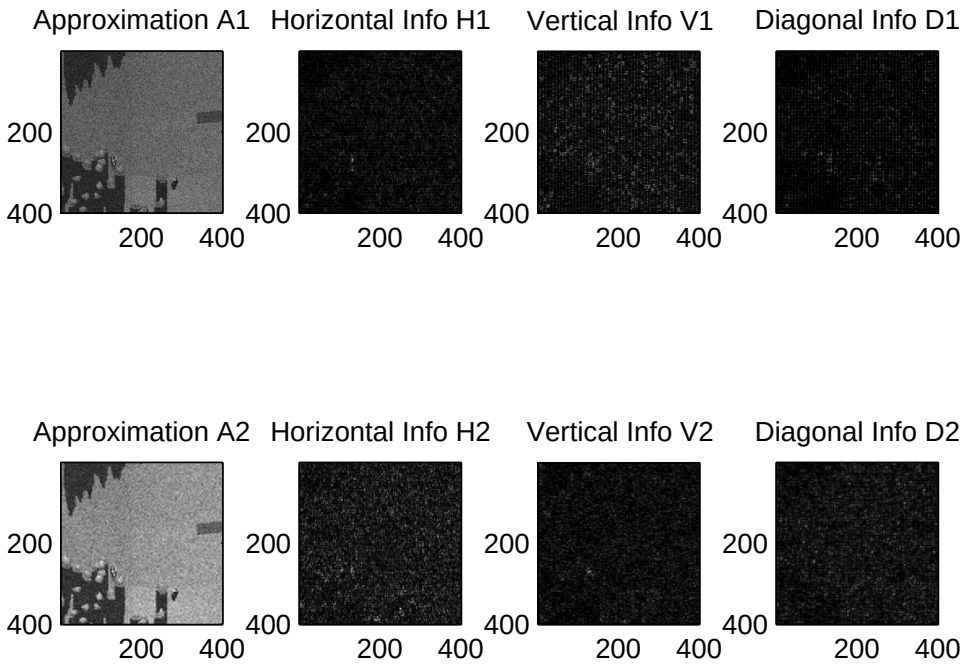

Figure 4.14: Using the Daubechies wavelet as a "mother" wavelet, image F_6 is broken down into two approximations so that compression can take place.

Once the reconstruction has occurred the two dimensional signal is represented as a series of wavelet coefficients and can be subjected to thresholding. A variety of threshold markers were set to obtain PSNR and MSE values for compression ratios ranging from 2:1 to 64:1, but for the purposes of analyzing the effect of the loss of data only three discrete values will be examined until the Section 4.4 of this chapter. While adding thresholds does cause the loss of data, there seems to be additional de-noising that occurs as well. Entropy in the data that causes distortions in other types of compressions does not occur as significantly in compression with WT algorithms. When a WT de-correlates the image pixels, it bins all the information contained in the image into the representative coefficients. Since white noise is uncorrelated, the transform does nothing to it. In the transform domain, the relevant image information that we

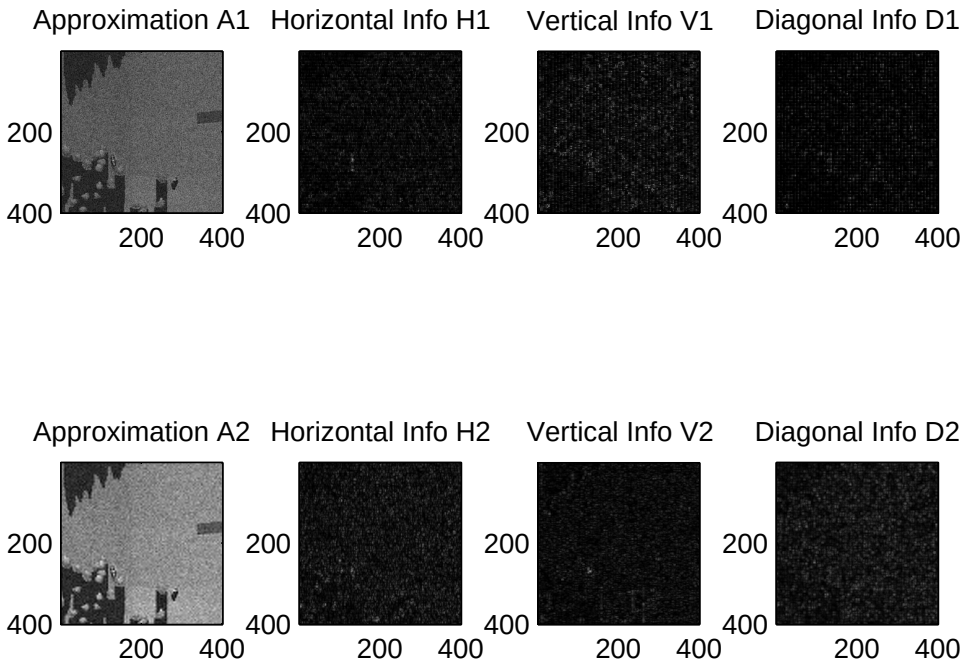

Figure 4.15: A second level deconstruction of image F_6 using bi-orthogonal wavelets.

consider important has a larger magnitude and can easily be separated from the noise data in the image. From the image analysis over many threshold values, applying a zero weight to the smaller wavelet coefficients will have a drastically greater affect on the noise than the actual image information itself. This results in a reconstructed image with some degradation but far less noise. This is first observed when comparing the change detection masks of an algorithm using wavelet based compression to even the normal data and will be supported with examples in the next section. With τ representing threshold, the following images represent both wavelet types at $\tau = 25, 50, 75$.

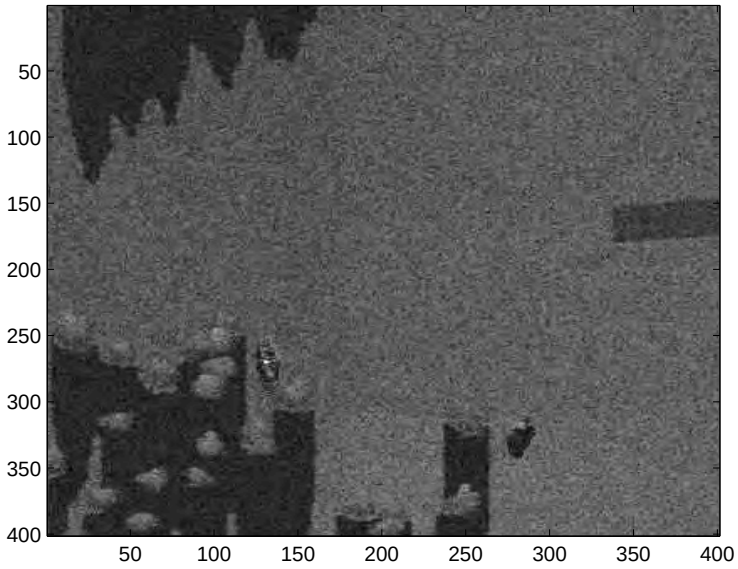

Figure 4.16: Daubechies WT compression with $\tau = 25$.

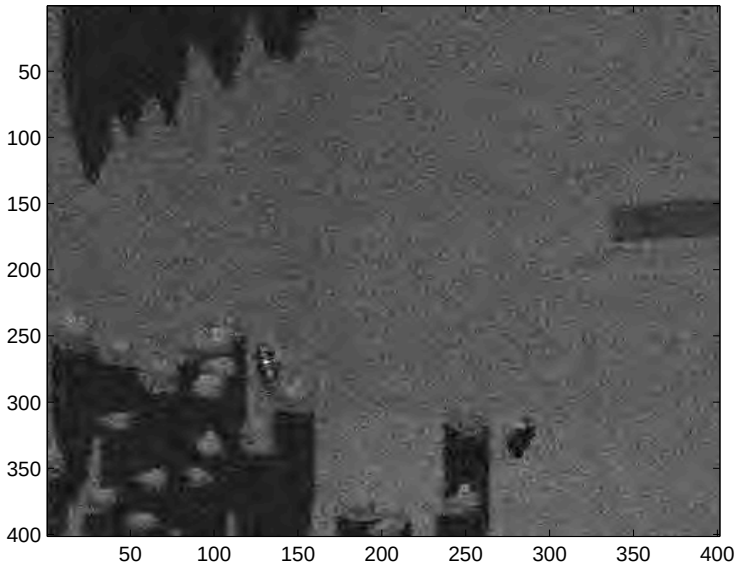

Figure 4.17: Daubechies WT compression with $\tau = 50$.

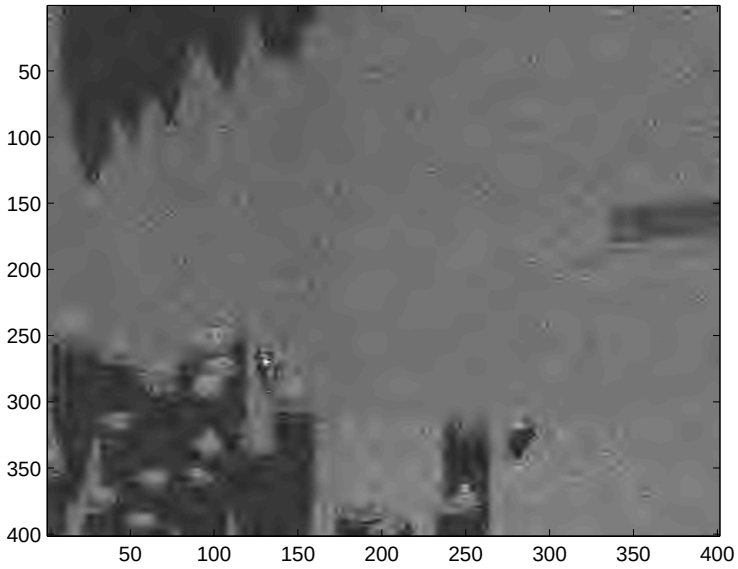

Figure 4.18: Daubechies WT compression with $\tau = 75$.

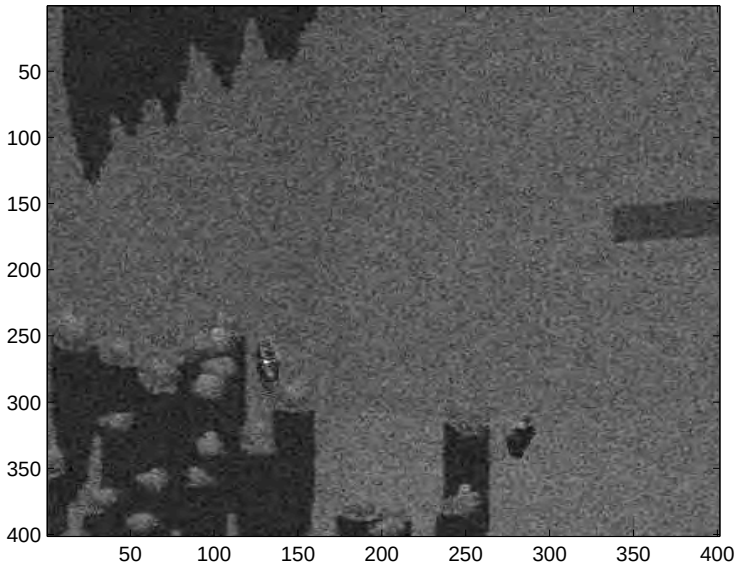

Figure 4.19: Bi-orthogonal compression with $\tau = 25$.

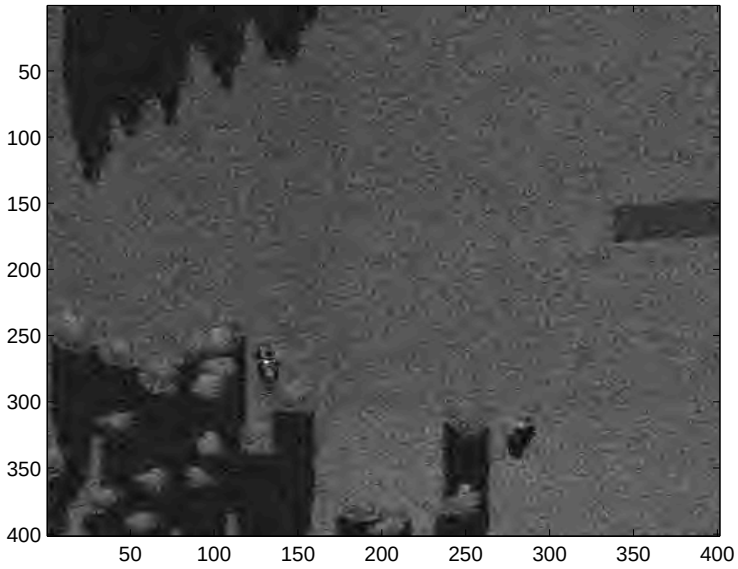

Figure 4.20: Bi-orthogonal compression with $\tau = 50$.

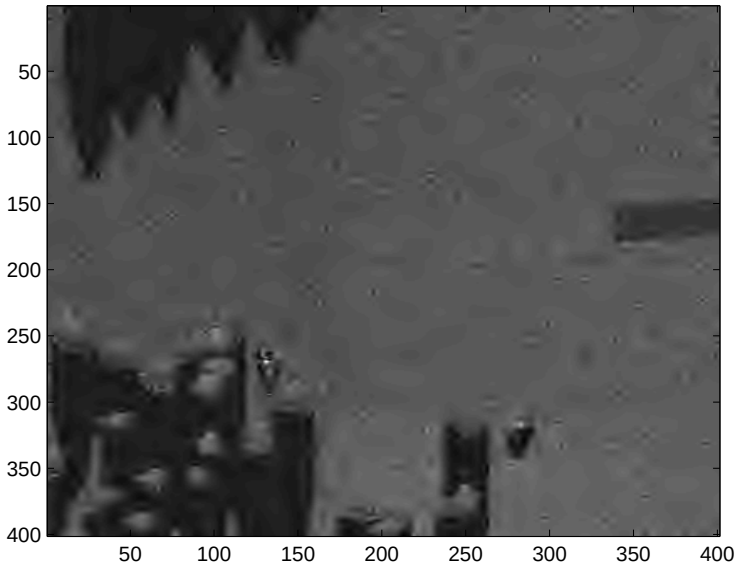

Figure 4.21: Bi-orthogonal compression with $\tau = 75$.

4.3 Post Compression CD Masks

After the compression of all ten images were processed with all 11 compression types and levels, change detection masks were created and compared to the original. In this section change detection in data set G_1 will be discussed because of the large amount of entropy in the system as well as the interesting effects that JPEG and the WT compression algorithms had on these two scenes.

In the hybrid SVD change masks, we have the de-noising factor that occurs as a result of the WT. However, as more coefficients are added, more noise gets added to the scene. The trade-off is that with more coefficients, there is less decomposition of the original image. The same holds true for the Daubechies and Bi-orthogonal wavelets. The only difference is the the magnitudes of information and noise that are present in each image, which will affect what is considered significant change. The JPEG change mask was quite different. As stated earlier, due to the amount of pixel padding when compression took place, there is a large number of pixels where change is detected that are clearly false positives. This is simply due to the way the algorithm works since all compression methods used the same change detection metrics outlined in Table 4.1. In most of the other scenes change was accurately detected with far less noise. While the JPEG compression technique had change detection in areas outside the expected areas in this scene its false positives in other scenes is far less significant although very much present. For more change detection masks from another scene selection please see Appendix A. For the JPEG algorithm, the change mask was recorded at an 8:1 compression ratio where there was a marked difference in the magnitude of padded pixels when compared to the 16:1 compression ratio.

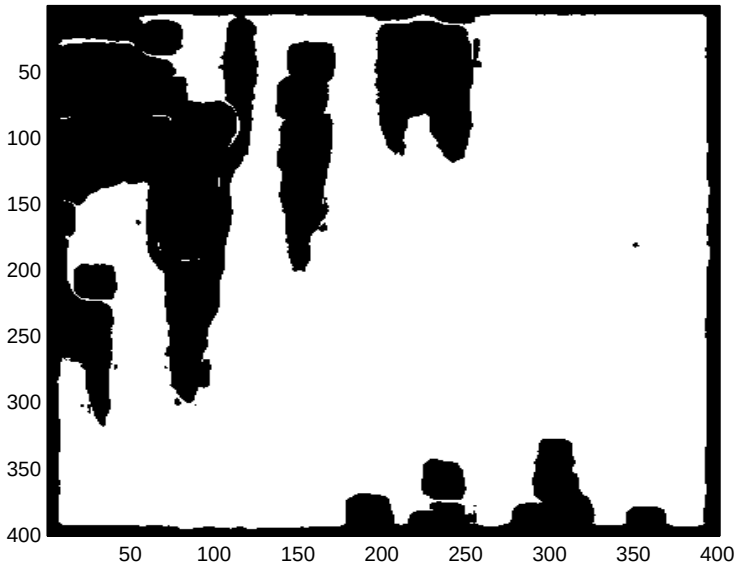

Figure 4.22: Change Mask for hybrid SVD_{25}.

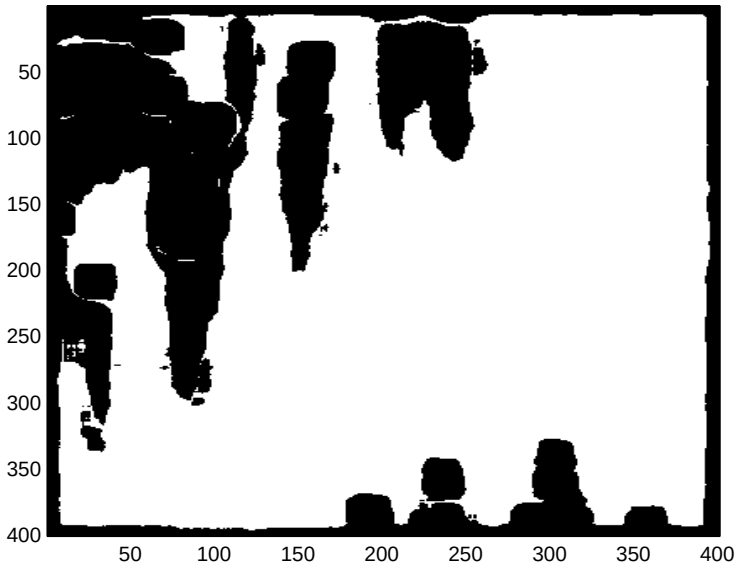

Figure 4.23: Change Mask for hybrid SVD_{50}.

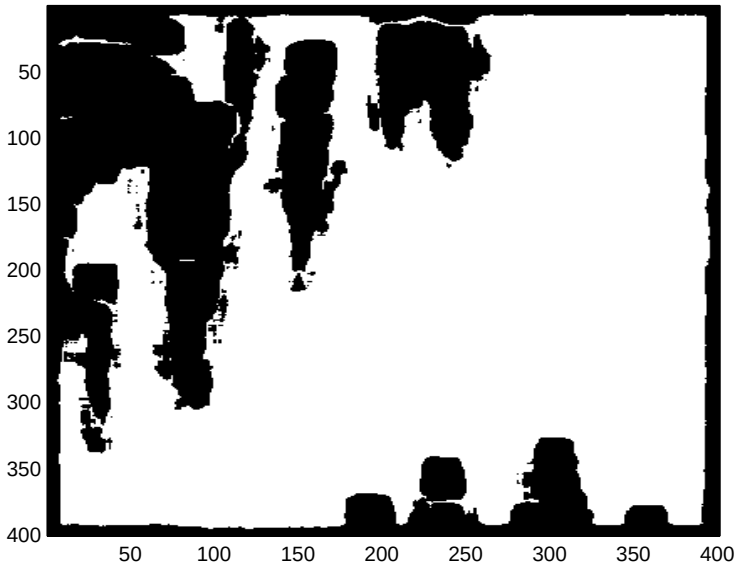

Figure 4.24: Change Mask for hybrid SVD_{75}.

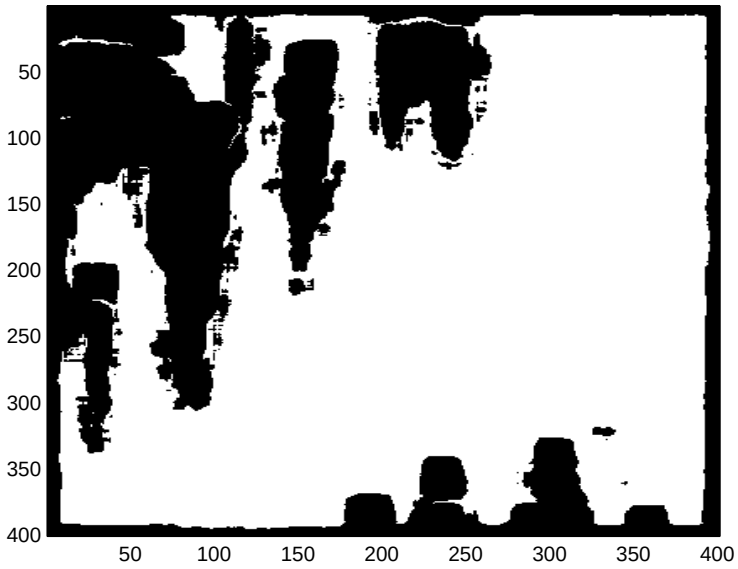

Figure 4.25: Change Mask for hybrid SVD_{100}.

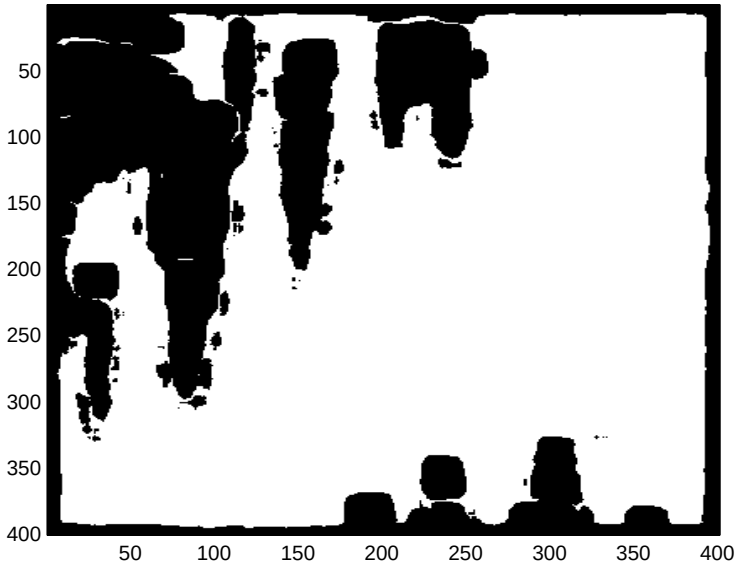

Figure 4.26: Change Mask for Daubechies WT with $\tau = 25$.

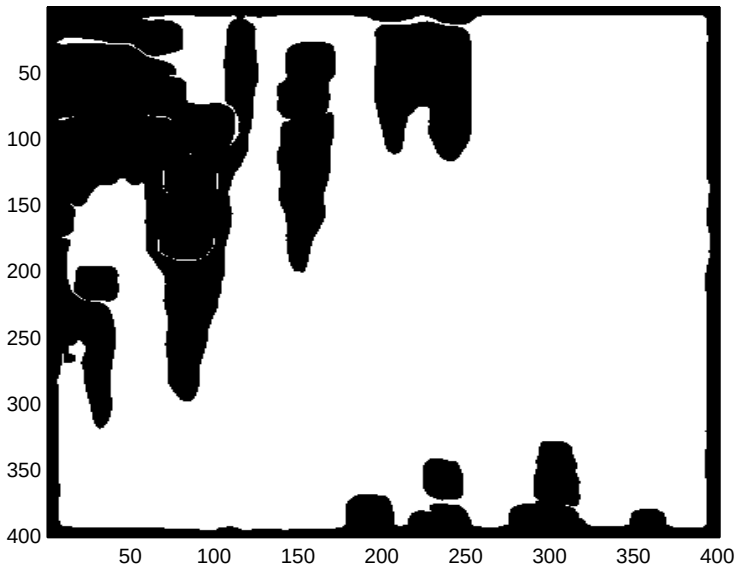

Figure 4.27: Change Mask for Daubechies WT with $\tau = 50$.

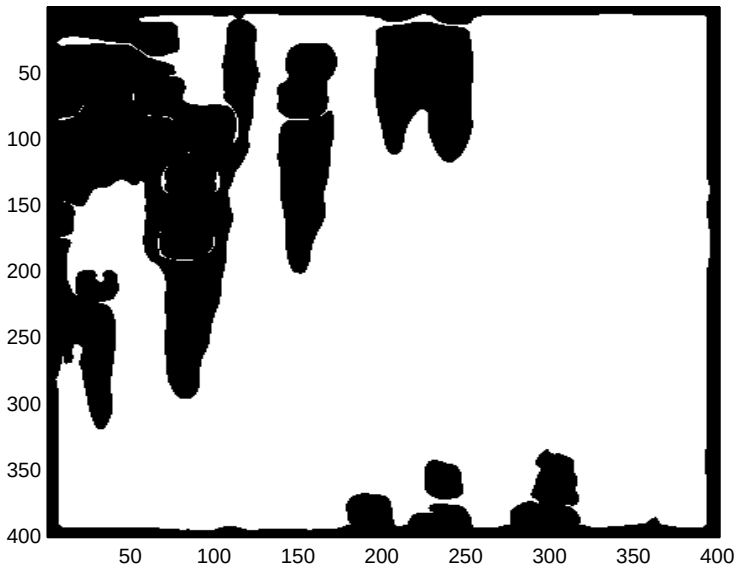

Figure 4.28: Change Mask for Daubechies WT with $\tau = 75$.

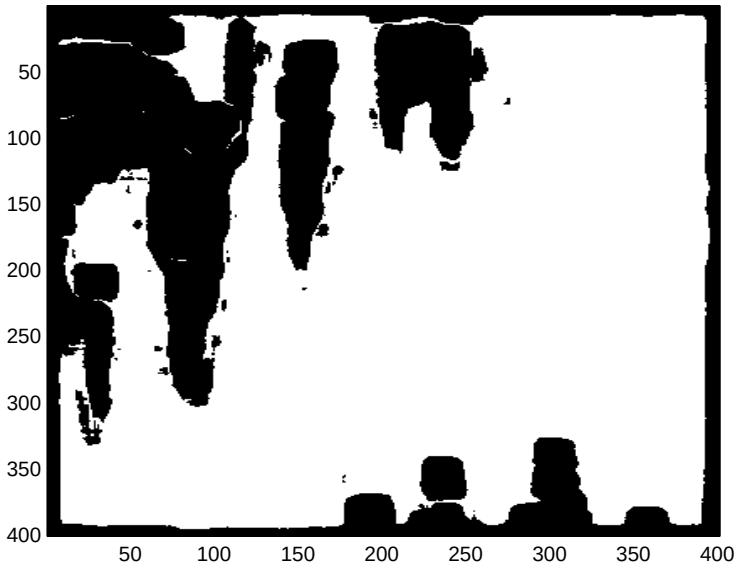

Figure 4.29: Change Mask for bi-orthogonal WT with $\tau = 25$.

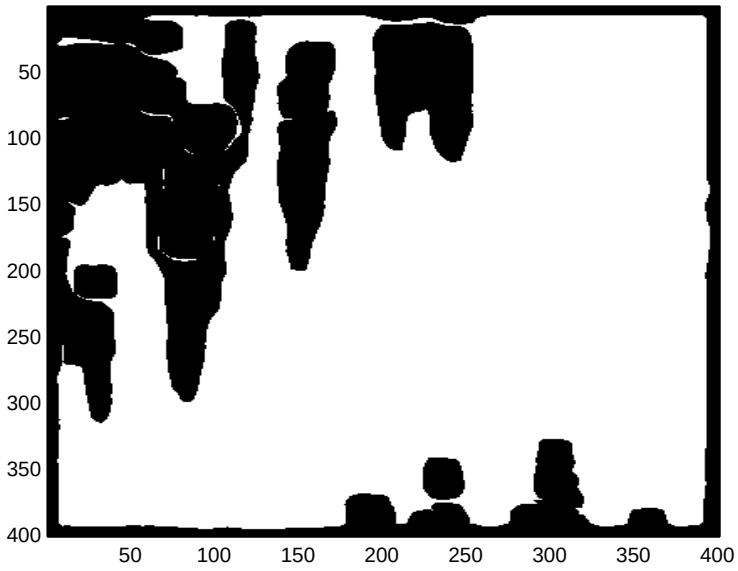

Figure 4.30: Change Mask for bi-orthogonal WT with $\tau = 50$.

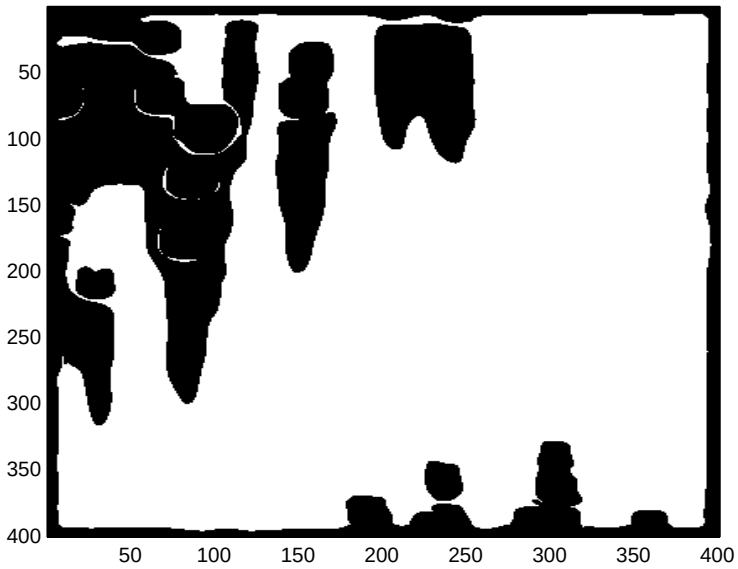

Figure 4.31: Change Mask for bi-orthogonal WT with $\tau = 75$.

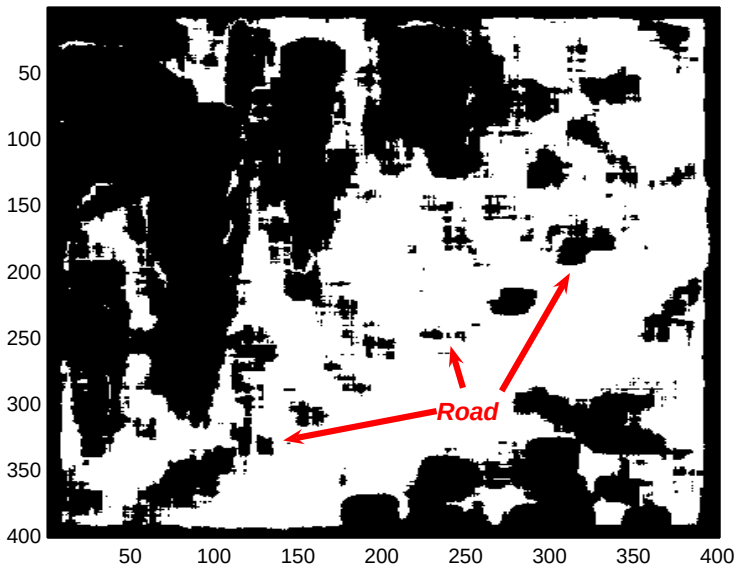

Figure 4.32: Change Mask for JPEG. While not present in other change masks, the JPEG compression caused the CD algorithm to recognize the parts of the road as significant change even though nothing had happened in the area.

4.4 Benchmarks

4.4.1 Compression Scores. Every one of the compression techniques was computed at various levels to see how PSNR was affected in order to further analyze which technique could produce the best image with the best compression ratio. Depending on the war-fighters' basic needs (in terms of compression), the algorithms with the best PSNR can be selected and used for change detection. For the purposes of comparison, a simple SVD algorithm was included to see the differences between it and the hybrid version. Both versions of the SVD algorithms were affected only minutely after a certain level of coefficients were removed which is supported by work done by Wang *et al.* [27]. One of the more surprising results is the rapid deterioration of the JPEG algorithm. After the compression ratio approached 16:1 there was a sharp drop-off making it fall below even standard SVD. It is for that reason that the 8:1 ratio was used in the study. After analysis of the data it was found that JPEG had the sharp drop-off due to the padding effect it had on the uncorrelated imagery.

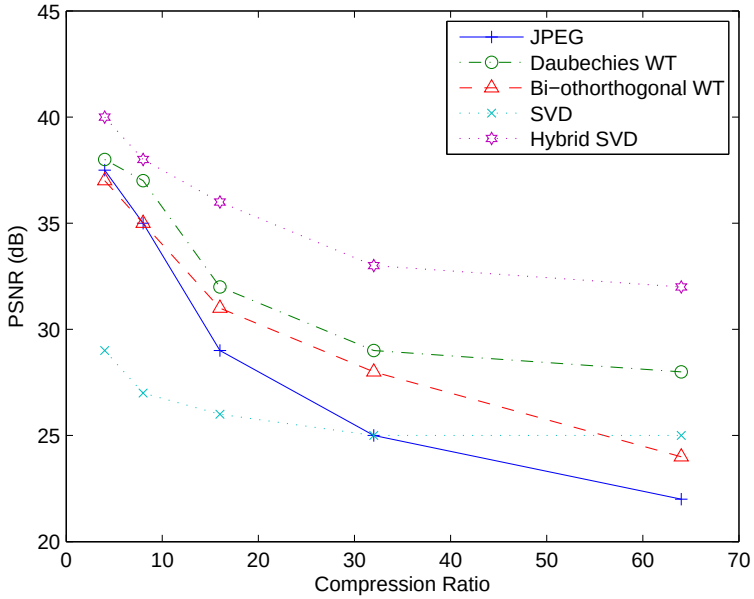

Figure 4.33: Each of the 5 compression algorithms were analyzed at 2^n levels where $n = 1, 2, ..., 6$. to find out how they compare to each other in terms of PSNR as the compression ratio increased.

Table 4.2: Compression Ratios by Algorithm.

Compression Type	Avg. Compression Ratio
Hybrid SVD_{25}	8.33:1
Hybrid SVD_{50}	4.21:1
Hybrid SVD_{75}	2.53:1
Hybrid SVD_{100}	2.13:1
Db_{25}	5.26:1
Db_{50}	15.76:1
Db_{75}	26.7:1
$Bior_{25}$	4.51:1
$Bior_{50}$	13.91:1
$Bior_{75}$	27.48:1
JPEG	8:1

Since the data was only referenced at certain thresholds and using certain quantization matrices, only a few points on this graph were analyzed. Table 4.2 shows the average compression ratios for all of the methods used in this study. Only an average was shown because the compression ratio varied by image when computed to four significant digits.

4.4.2 CD Compression Analysis. After all the masks are made, the final metric of analysis for this research is to see how the change detection mask of the compressed data compares to the mask of the original data. The best way to analyze and compare this data is by using Receiving Operating Characteristic (ROC) plots. Each graph plots the compression points with the probability of false positive as the independent variable and the probability of detection as the dependant variable. Each scene has its own plot so that analysis by environment can be made. The SVD compression levels shown in each one of the ROC plots refer to the hybird algorithm.

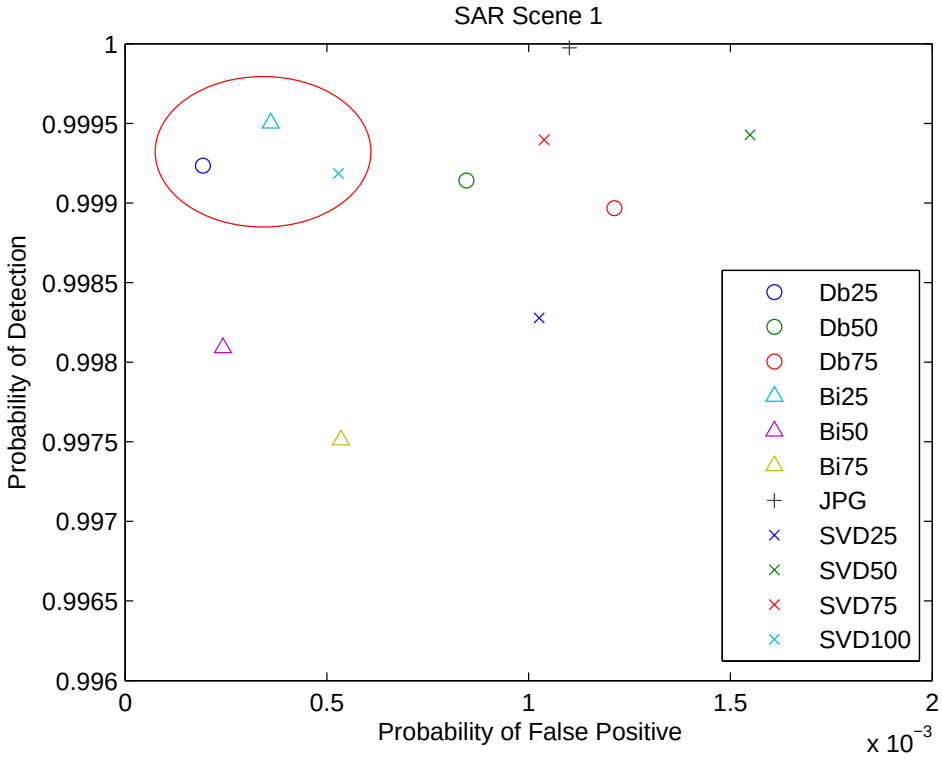

Figure 4.34: ROC of mask set D_1. The best three compression types are circled in red. In scene one Daubechie's WT with $\tau = 25$, Bi-orthogonal WT with $\tau = 25$ and SVD with 100 dominant elements are the best compression types.

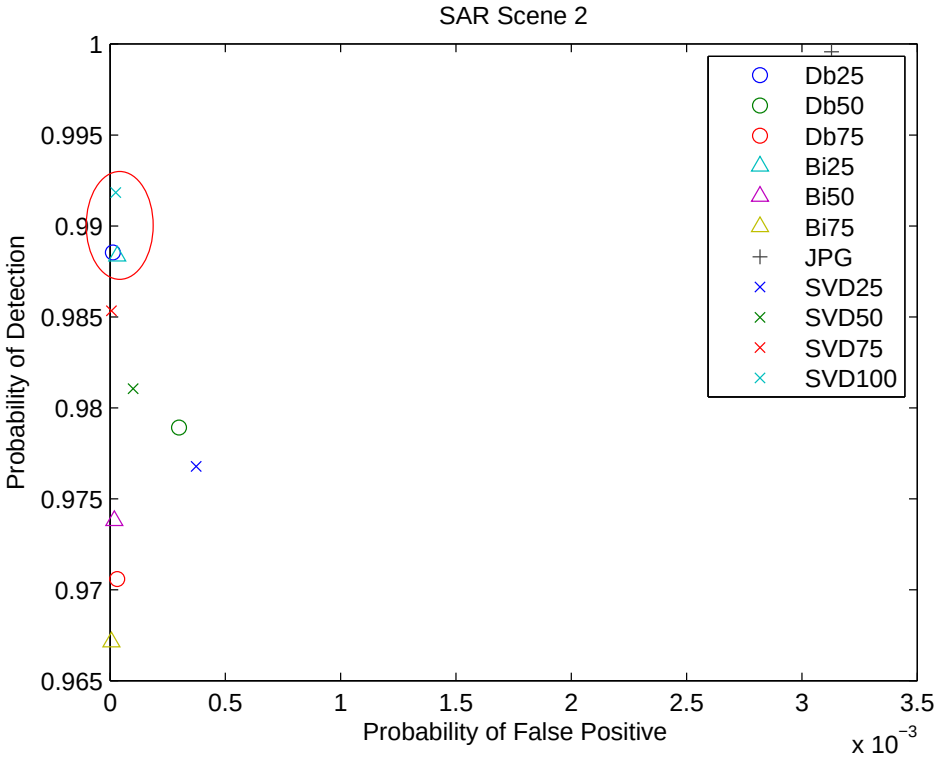

Figure 4.35: ROC of mask set F_1. In scene two Daubechie's WT with $\tau = 25$, Bi-orthogonal WT with $\tau = 25$ and SVD with 100 dominant elements again are the best compression types..

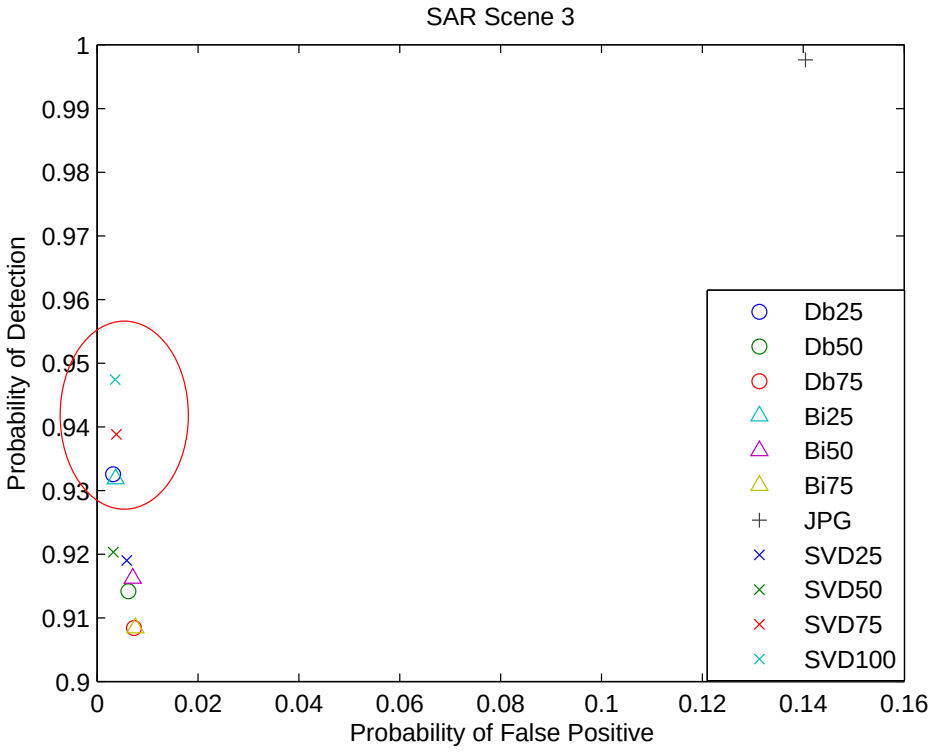

Figure 4.36: ROC of mask set G_1. In scene three SVD with 75 and 100 dominant elements perform the best while Daubechie's WT with $\tau = 25$, Bi-orthogonal WT with $\tau = 25$ are close behind.

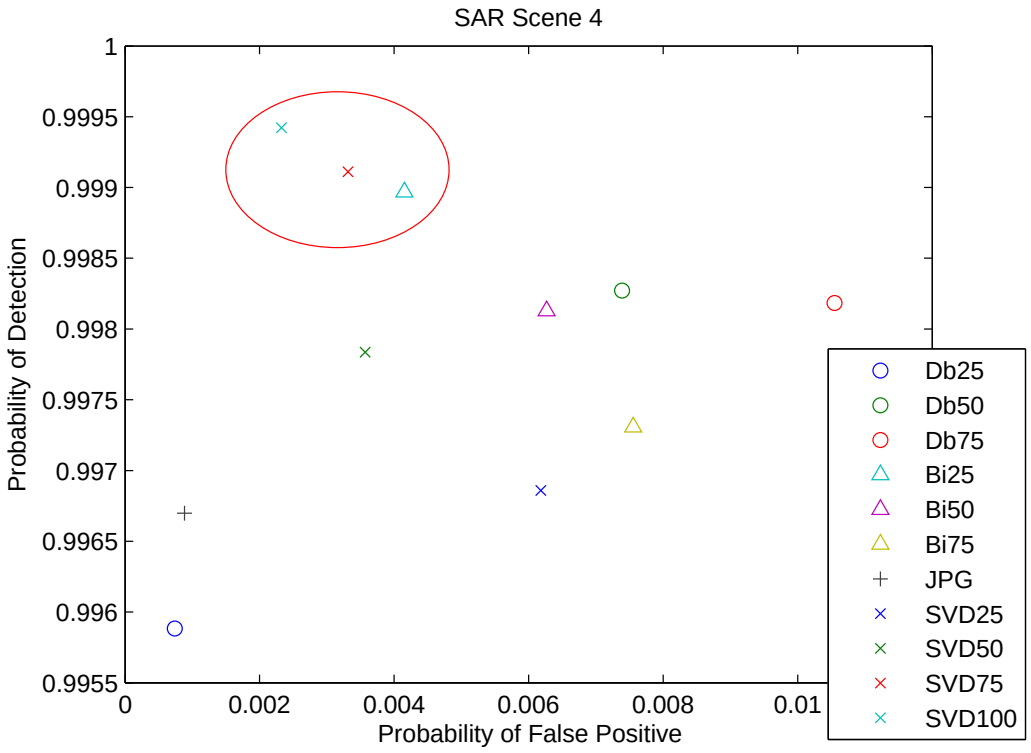

Figure 4.37: ROC of mask set G_2. In scene four there is a decision to be made on whether the probability of detection is more important then a high or low probability of false positive. If a lower probability of detection is acceptable, then JPEG could be considered the best compression algorithm. Otherwise the SVD algorithms with 75 and 100 dominant elements followed by the Bi-orthogonal WT with $\tau = 25$ are the best to use.

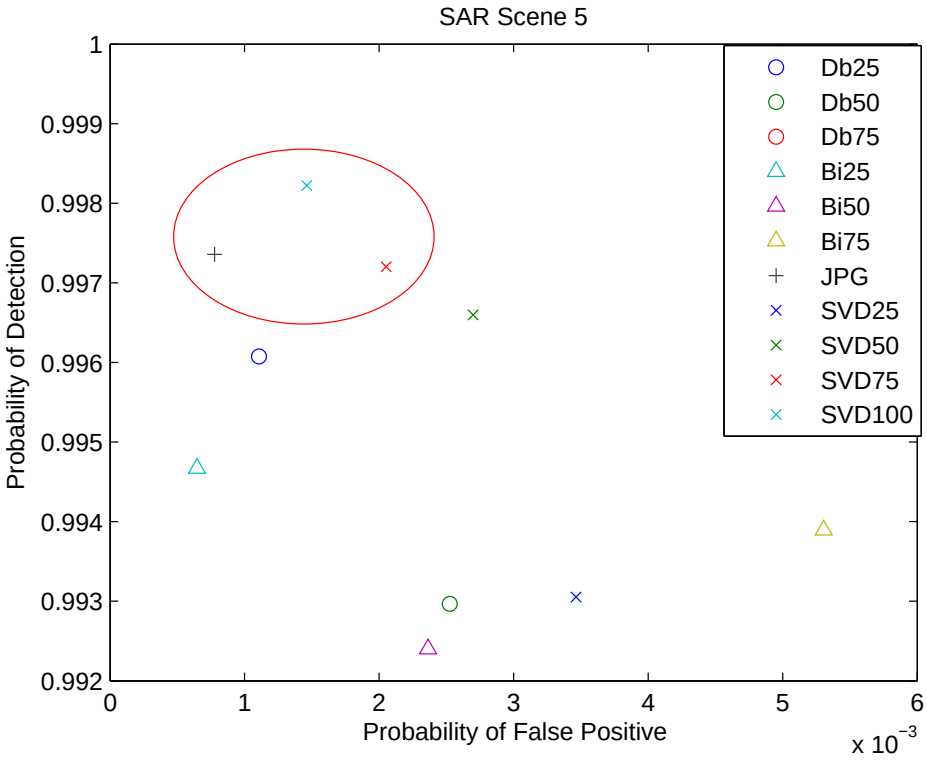

Figure 4.38: ROC of mask set Y_1. In scene five, JPEG is surprisingly clearly the best algorithm to use while SVD algorithms with 75 and 100 dominant elements performed almost as well.

In scene D_1 (Figure 4.34) both wavelet transforms, with a threshold of 25 perform the best with the hybrid-SVD_{100} algorithm performing almost as well . In every scene these three compression methods are the best except for area Y_1 (Figure 4.38), in which JPEG can be considered an alternative based on which what level of false positives is desired. In all other cases the JPEG algorithm performs well on the probability of detection, however, the chance that the detection is a false positive is also higher than all other algorithms. If one compression algorithm had to be chosen for all scenarios, the hybrid-SVD_{100} offers the best all around performance. In some cases the hybrid-SVD_{75} performed better than WT compression techniques. The fact that each of these compression algorithms produced different results in different environments supports the hypothesis that environment does play a factor in choosing a compression algorithm. Each environment does have a certain associated range of entropy to it [7], which is the primary reason for the difference in performance.

4.4.3 Environmental Analysis. Analyzing the ROC curves may determine which of the following compression methods is the optimal choice for each scene. It is the goal of this study to base the decision for a compression algorithm on not only the performance from the ROC plots, but also on the level of compression that can be achieved. Table 4.3 lists each scene, its three best compression algorithms based on the ROC plots and the compression ratios achieved by each type using the algorithms outlined in Chapters 2 and 3. The compression ratios seem to fall in line with other research studies using the same methods [5, 7, 20], however, the other studies never bench-marked the methods to a certain application. While there is a baseline set for which compression method would be used in each scenario, the amount of data processed in this research effort is quite small. The need for further processing would be necessary before being able to generalize one type of compression method to a type of environment.

4.4.4 Data Retention Analysis. The need to transfer an entire set of images is not needed if change detection is performed on board the collection platform.

While the first image in a series of geo-registered data would have to be kept in its entirety, each subsequent image would only need the pixels in which significant change was detected to be transferred across the communications link. Regardless of how much change is detected in the scene this can reduce the amount of information being sent. This analysis could allow the re-encoding of the image with a loss-less technique allowing further compression of the images. Table 4.3 shows the fraction of information that would need to be sent for the changed image in relation to the original for the normal data as well as each of the compressions analyzed in this study. Each one of these percentages are based on the 400×400 pixel array that were originally measured and analyzed in this chapter. This post processing step would help reduce the amount of data being sent by encoding every pixel mapping that doesn't have significant change detected with a zero. By adding all those zeros to the data, there is significantly less entropy, less "leaves" (in terms of entropy encoding) and hence less codewords assigned. From Table 4.4 the maximum amount of data that would be required to be sent from the second image is only 51.05% which gives us a secondary compression ratio of 1:1.9. On the other extreme in areas like D_1 where the only

Table 4.3: Optimal Compression by Area.

Set	Images	Environment	Compression Type	Compression Ratio
D_1	2,3	Desert	Daubechies WT, $\tau = 25$	5.28:1
			Bi-orthogonal WT, $\tau = 25$	4.53:1
			SVD_{100}	2.16:1
F_1	6,7	Forest,	SVD_{100}	2.13:1
		Plains, and	Daubechies WT, $\tau = 25$	5.25:1
		Tarmac	Bi-orthogonal WT, $\tau = 25$	4.49:1
G_1	2,3	Forest	SVD_{100}	2.09:1
			SVD_{75}	2.45:1
			Daubechies WT, $\tau = 25$	5.22:1
G_2	5,6	Forest	SVD_{100}	2.12:1
		and	SVD_{75}	2.45:1
		Tarmac	JPEG	8:1
Y_1	12,13	Plains	SVD_{100}	2.15:1
			JPEG	8:1
			SVD_{75}	2.47:1

change was the movement of a few vehicles, the percent of pixels that had change detected was as little as 0.69% which allows compression as high as 138.8:1. This method only looks at the removal of redundant information in the SAR imagery, but application of this technique to the phase history is also possible.

Table 4.4: Percent of Data Retention Required.

Compression Style	Percent of Data with CD				
	D_1	F_1	G_1	G_2	Y_1
Uncompressed	0.89	30.03	37.24	8.58	14.87
Bi-orthogonal WT, $\tau = 25$	0.87	28.87	30.79	8.89	14.41
Bi-orthogonal WT, $\tau = 50$	0.72	27.41	29.57	9.02	14.35
Bi-orthogonal WT, $\tau = 75$	0.69	26.74	28.84	9.07	14.79
Daubechies WT, $\tau = 25$	0.83	28.88	30.81	8.24	14.59
Daubechies WT, $\tau = 50$	0.89	27.95	29.28	9.15	14.42
Daubechies WT, $\tau = 75$	0.91	27.09	28.81	9.45	15.51
Hybrid SVD_{25}	0.82	27.74	29.73	8.88	14.53
Hybrid SVD_{50}	0.99	28.14	29.59	8.72	14.80
Hybrid SVD_{75}	0.93	28.56	31.50	8.82	14.80
Hybrid SVD_{100}	0.86	29.21	32.34	8.76	14.84
JPEG	1.00	30.30	51.05	8.34	14.69

V. Conclusion

5.1 Benefits of this Research

Given the experimental results of this research effort, it is concluded that lossy compression along with relevant data retention methods can be used to significantly decrease the sizes of SAR imagery. In four of the five scenes hybrid SVD using wavelet transforms has proven to be the best at performing change detection analysis with a low probability of false information. In the one scene where it did not, it was only behind two compression methods using Daubechies and bi-orthogonal wavelets which had extremely low thresholds.

In addition it is found that using two different change detection algorithms set at different threshold values acting in conjunction with each other will create a better change detection mask. The change detection masks often yielded the best results when a combination of the statistical Gaussian method was used with the likelihood ratio test. Items that were man-made like roads and vehicles seemed to require a much lower threshold value than environmental changes such as tree movement and removal. However increasing the threshold factor of one had a direct correlation with the amount of false hits that would occur. By allowing two different algorithms to form a binary union to create one change detection mask, even the most minute changes in each scene were detected with decreased error.

Environment played a huge factor in affecting how effective the algorithms were once compression occurred. While the hybrid SVD performed significantly well across the board, wavelet transform based compression seemed to do best in forest imagery and scenes with increased entropy. JPEG algorithms performed well in areas of minute change and low entropy in the image.

The ultimate goal of this research was to find empirical proof of compression methods that could work with certain change detection algorithms so that one day, this entire process could be automated to the point where a machine could determine whether or not data was relevant to the war-fighter. With the abundance of data created by remote sensing platforms, it is more and more necessary to be able to

process only the data that is important and this research has taken the first steps to create a system that will automate this requirement. While the results are promising, there are several more things that could be done to achieve this end goal.

5.2 Recommendations for Future Work

While working on this research, several limitations occurred as well as additional insights made that are recommended for future efforts. These areas are:

1. Increase the size of the environmental data range by including urban landscapes.
2. Expand the relevant data retention methods to include not only the image backscatter, but the corresponding phase history as well.
3. Move past synthetic phase history to real data, where speckle, motion blurring, and other SAR artifacts that add additional noise to the image are considered in compression algorithms and detection coding.
4. With real data acquired, apply the same theories with coherent change detection. Real data will have areas where backscatter have the same intensity values but have unequal phases.
5. As technology pushes forward, so must the research with new compression schemes and detection methods. Adaptation of more recent innovations in compression such as the final specifications for JPEG-2000 and the continuation of the pursuit of lossless methods that yield better compression ratios is needed.
6. Study the effects of compression of geo-registration. Since all the examined data was synthetic and pre-registered, this was never an issue, but with real data it could lead to potential problems.

Appendix A. Additional Compression and CD Mask Data

Since only one to two images were given as examples for each of the sections in Chapter 4, Appendix A will include images from Area F with all the compression techniques applied. All compressed data here is presented in the range given by Table 4.1.

A.1 Compressed Data

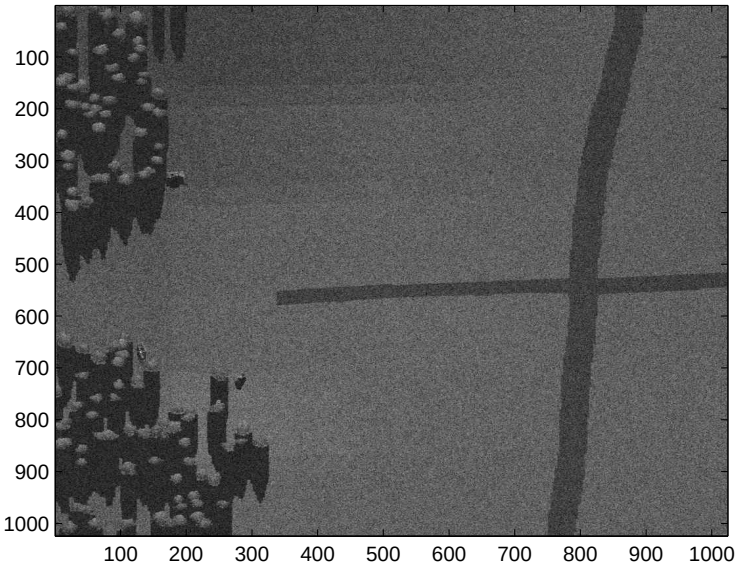

Figure A.1: The uncompressed image F_6

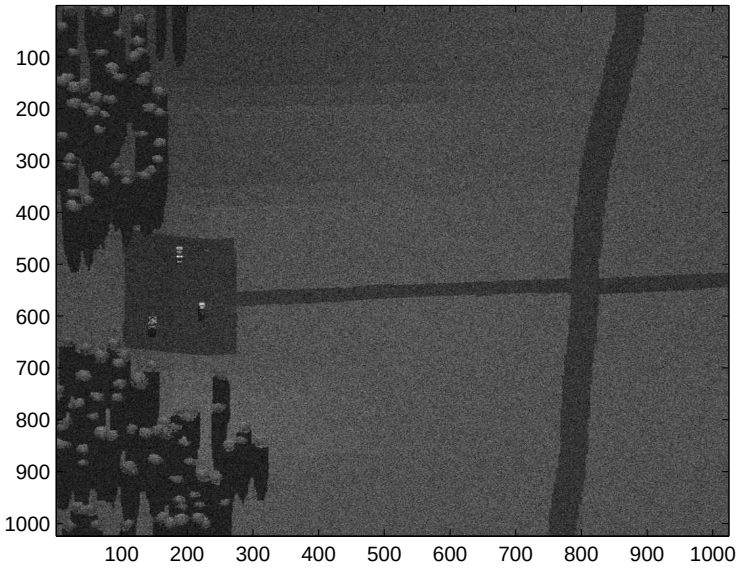

Figure A.2: The uncompressed image F_7

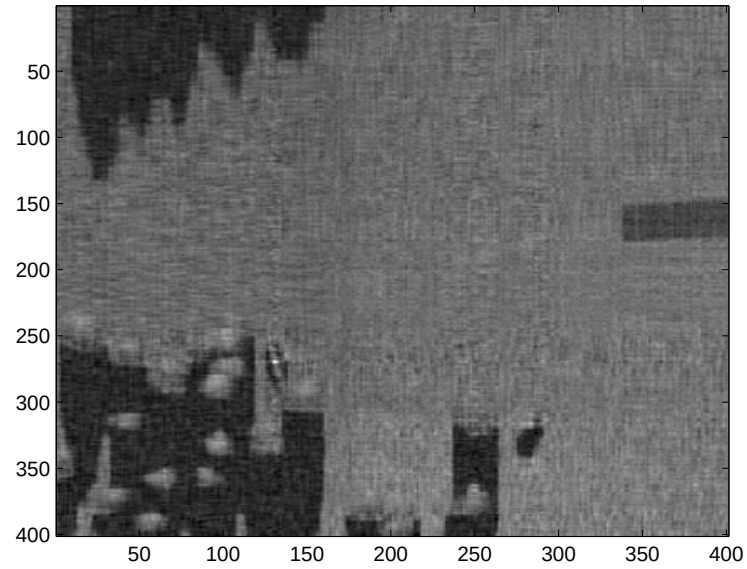

Figure A.3: Hybrid SVD_{25} F_6

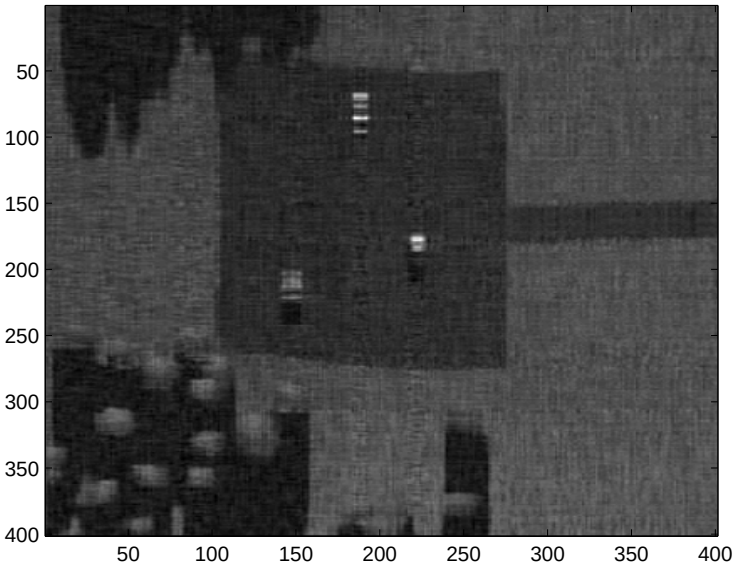

Figure A.4: Hybrid SVD_{25} F_7

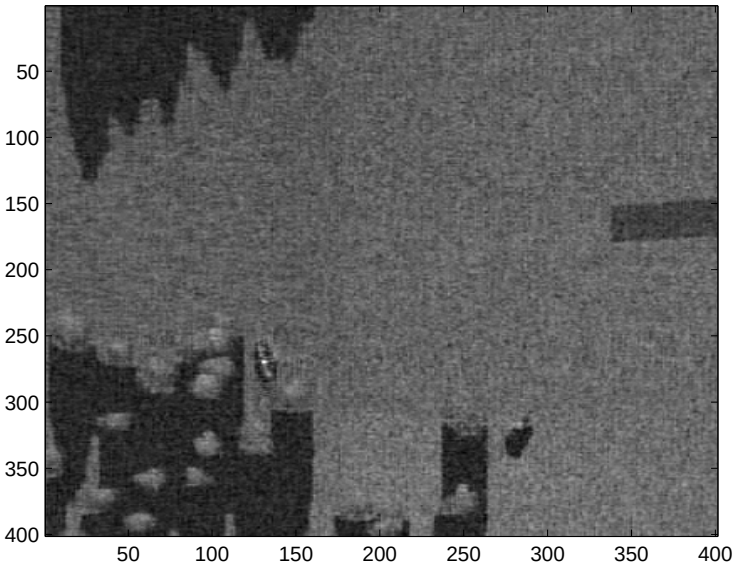

Figure A.5: Hybrid SVD_{50} F_6

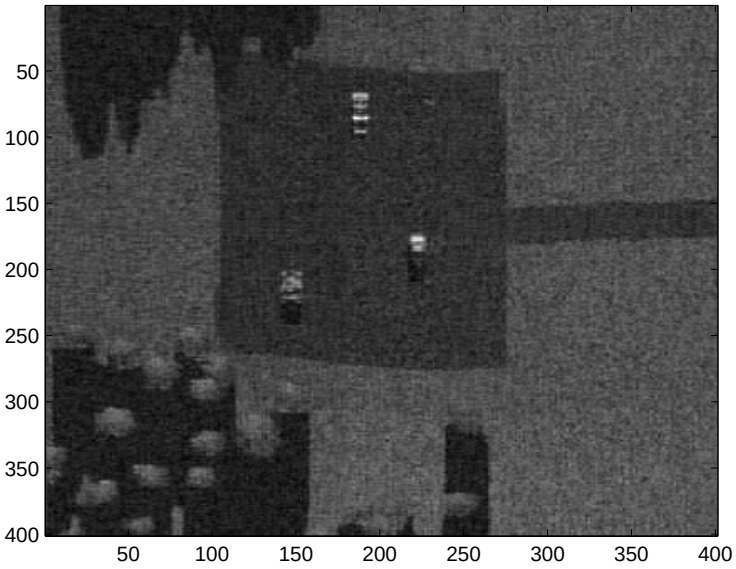

Figure A.6: Hybrid SVD_{50} F_7

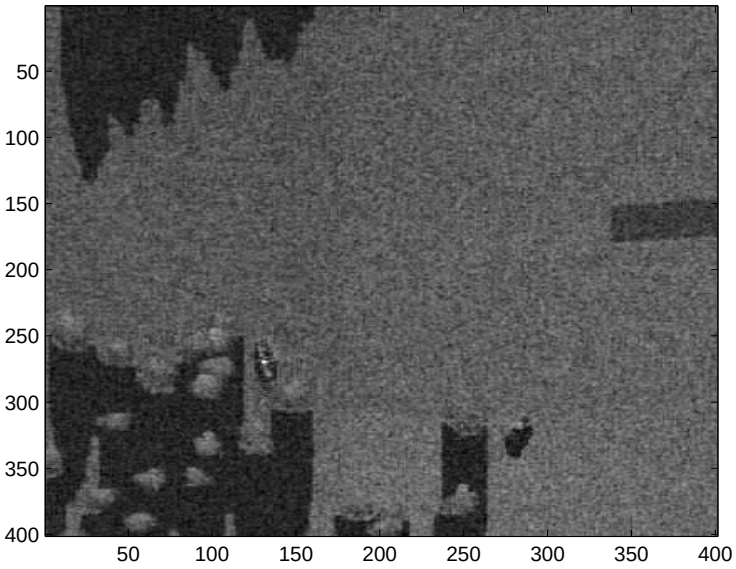

Figure A.7: Hybrid SVD_{75} F_6

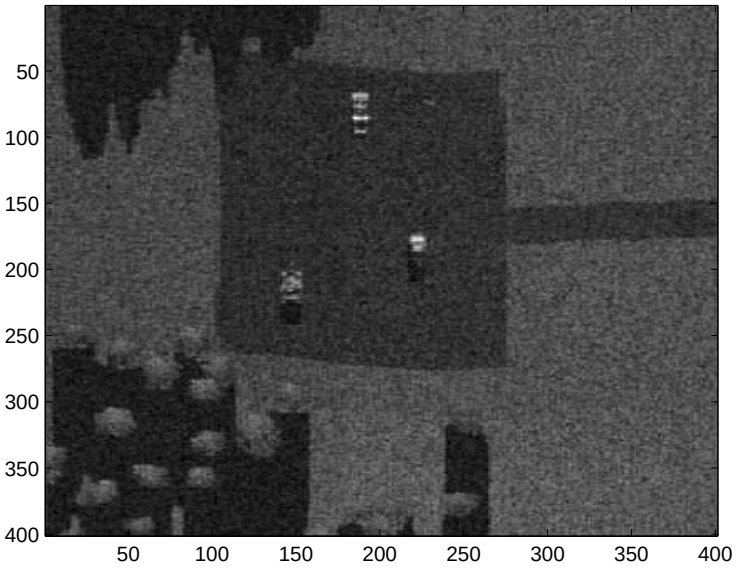

Figure A.8: Hybrid SVD_{75} F_7

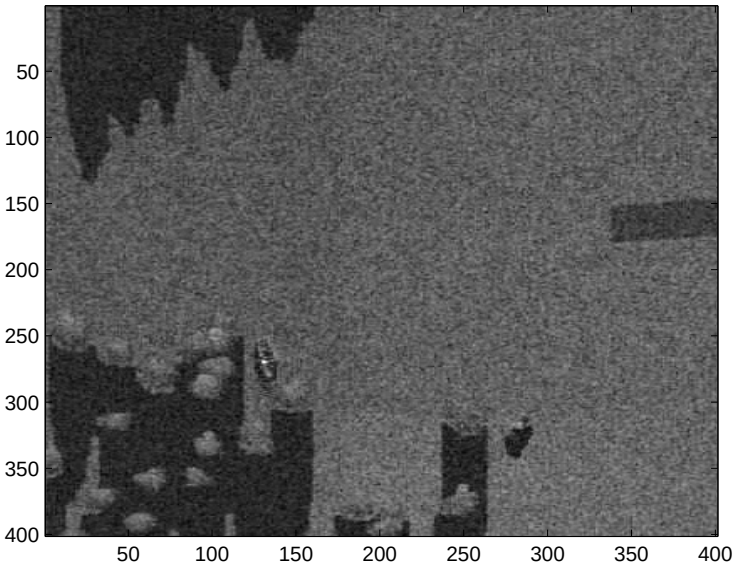

Figure A.9: Hybrid SVD_{100} F_6

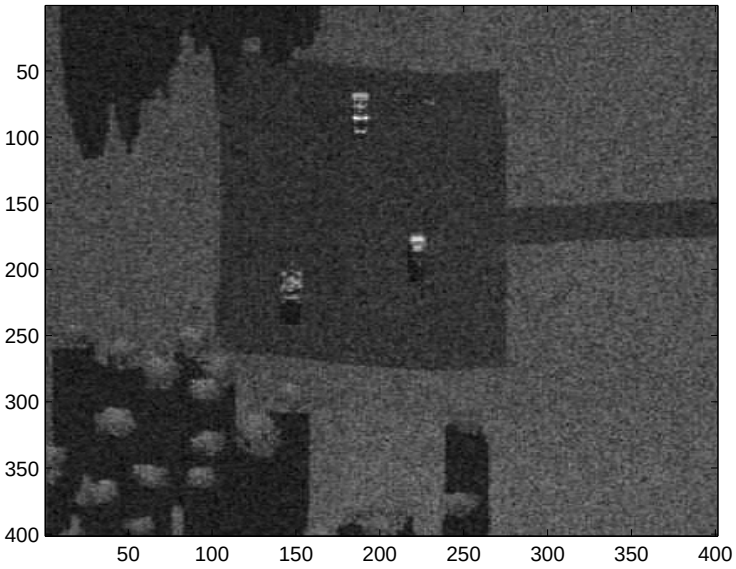

Figure A.10: Hybrid SVD_{100} F_7

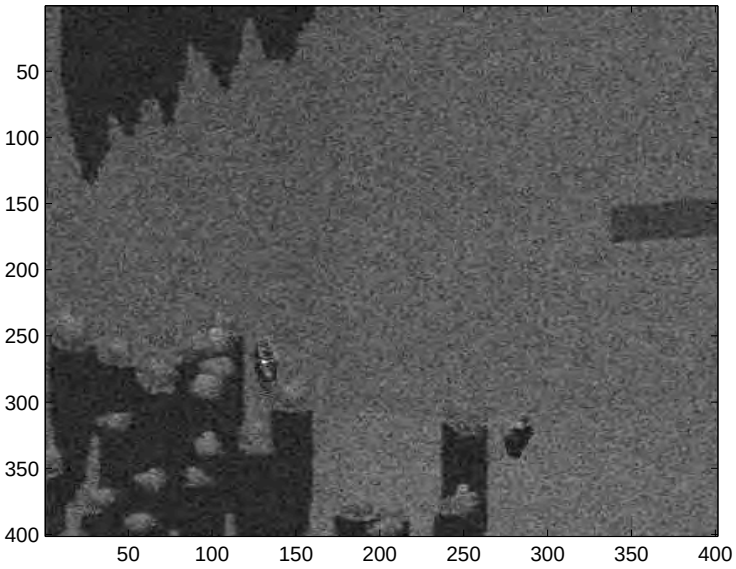

Figure A.11: Bi-orthogonal WT of F_6 with $\tau = 25$

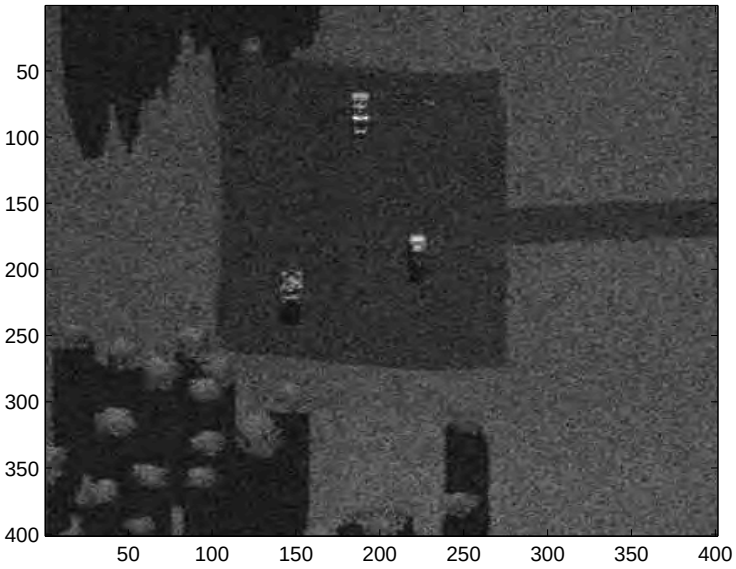

Figure A.12: Bi-orthogonal WT of F_7 with $\tau = 25$

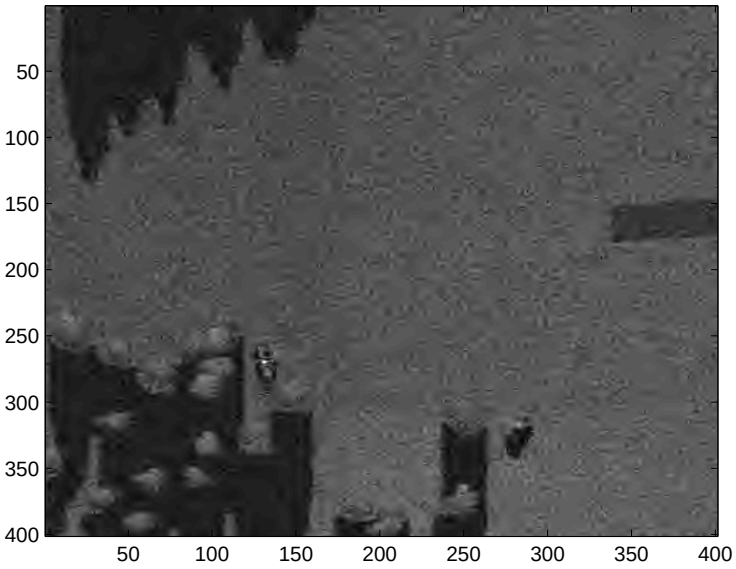

Figure A.13: Bi-orthogonal WT of F_6 with $\tau = 50$

Figure A.14: Bi-orthogonal WT of F_7 with $\tau = 50$

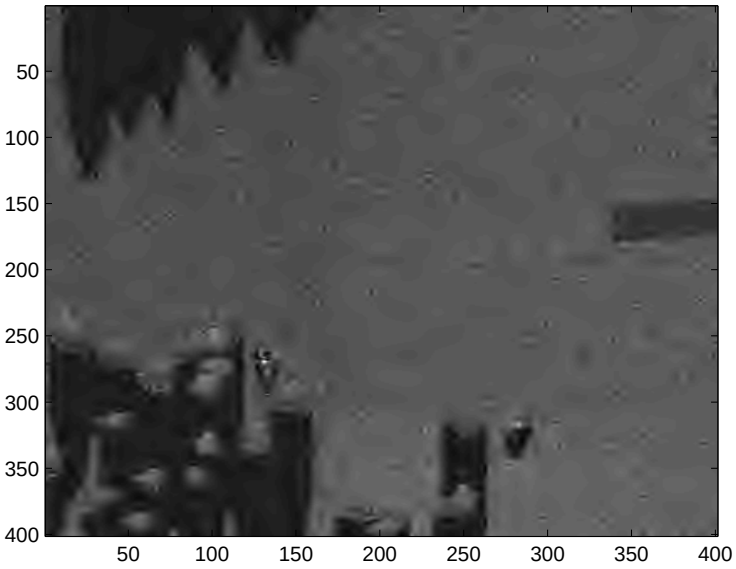

Figure A.15: Bi-orthogonal WT of F_6 with $\tau = 75$

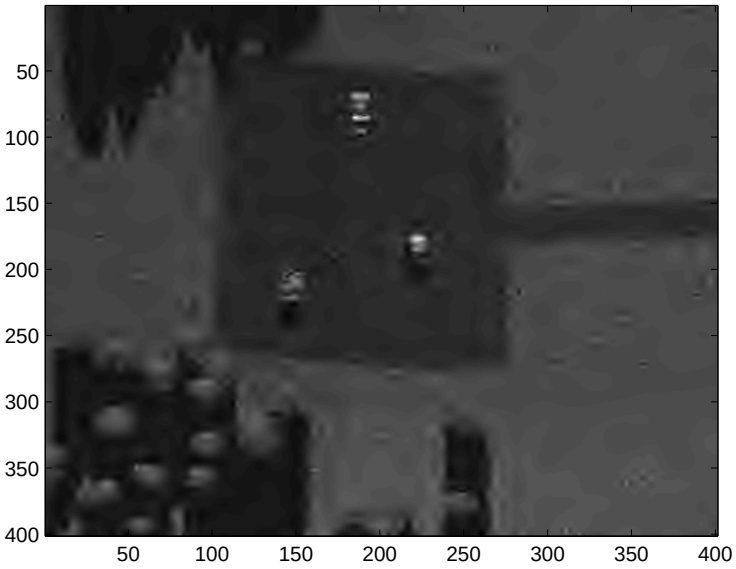

Figure A.16: Bi-orthogonal WT of F_7 with $\tau = 75$

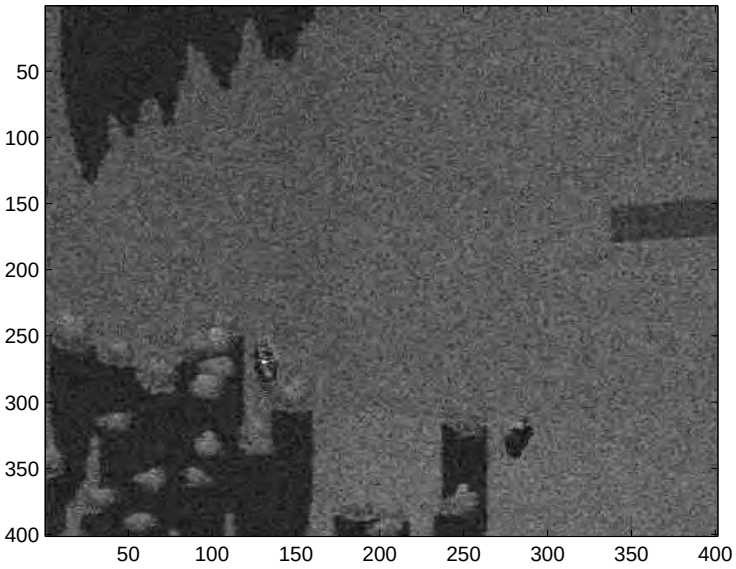

Figure A.17: Daubechies WT of F_6 with $\tau = 25$

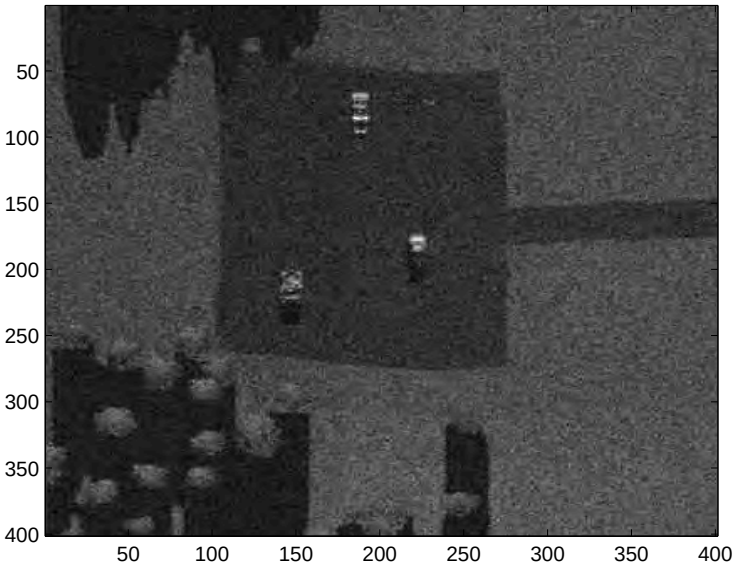

Figure A.18: Daubechies WT of F_7 with $\tau = 25$

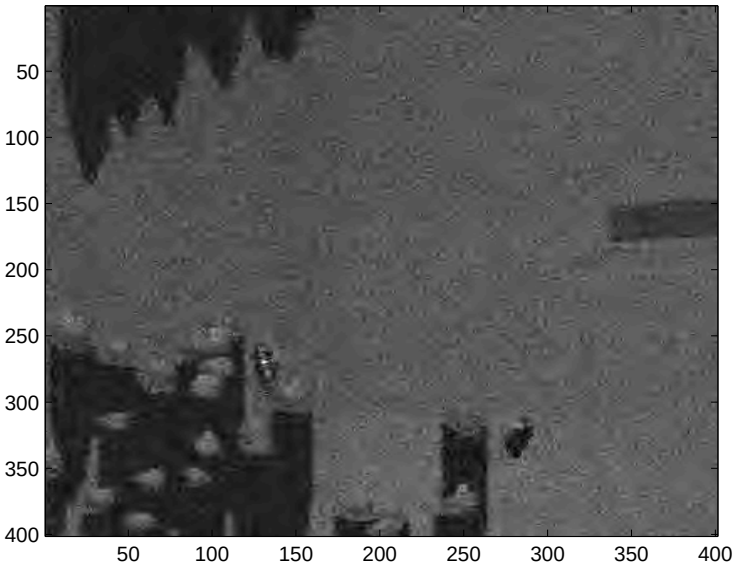

Figure A.19: Daubechies WT of F_7 with $\tau = 50$

Figure A.20: Daubechies WT of F_7 with $\tau = 50$

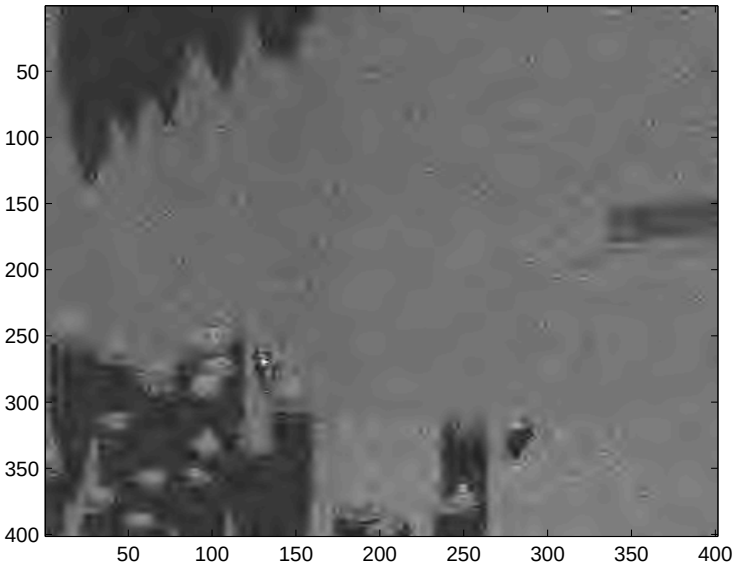

Figure A.21: Daubechies WT of F_6 with $\tau = 75$

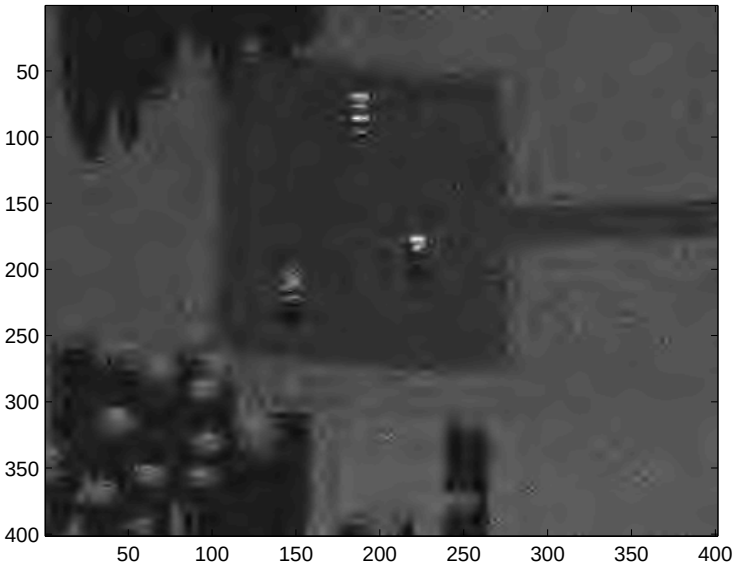

Figure A.22: Daubechies WT of F_7 with $\tau = 75$

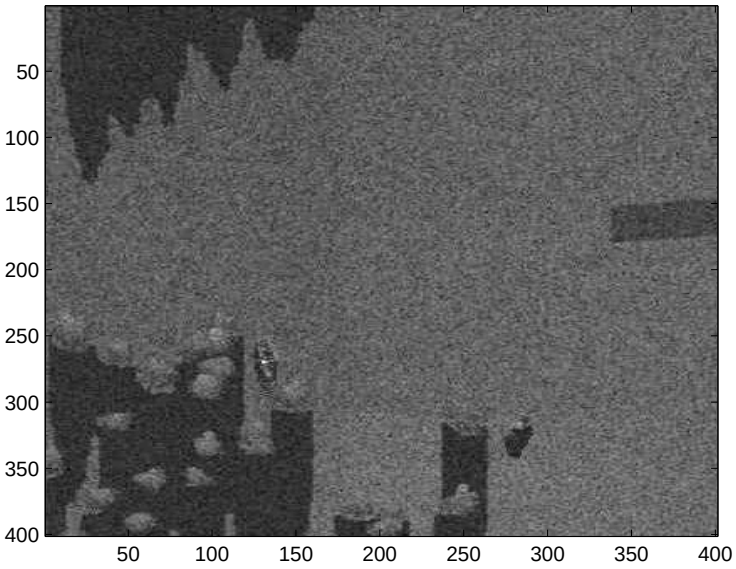

Figure A.23: JPEG of F_6

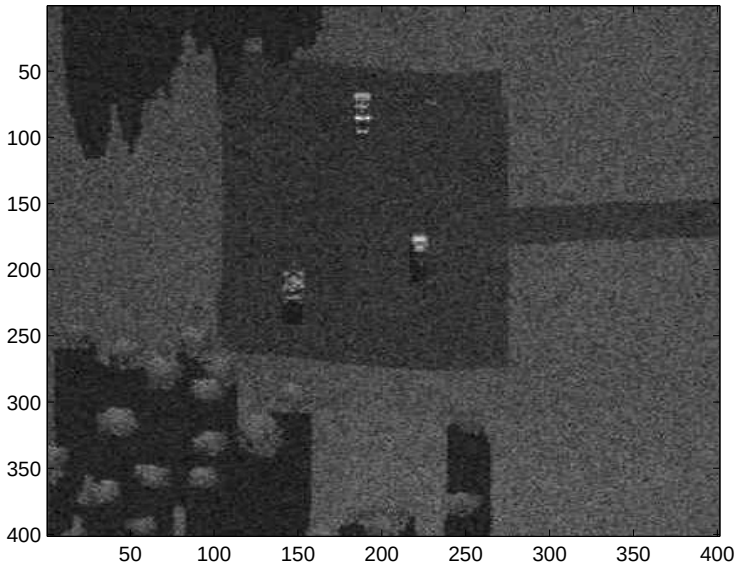

Figure A.24: JPEG of F_7

A.2 CD Masks for Area F

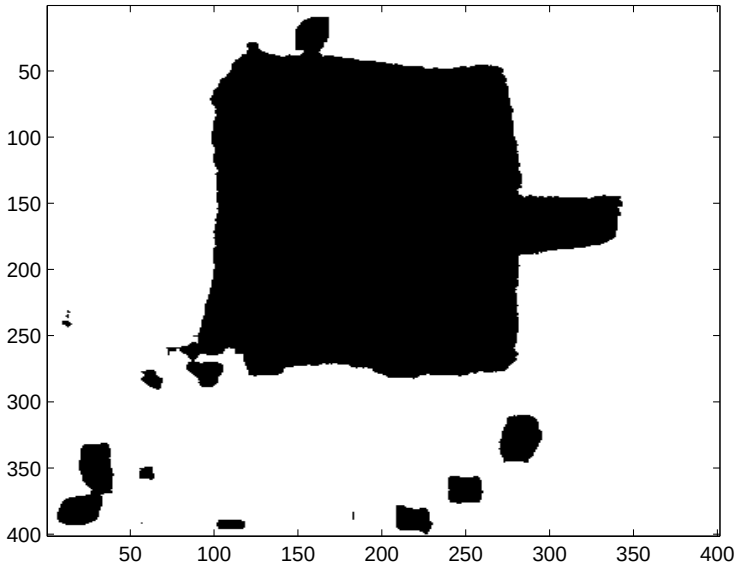

Figure A.25: Uncompressed change mask for Area F

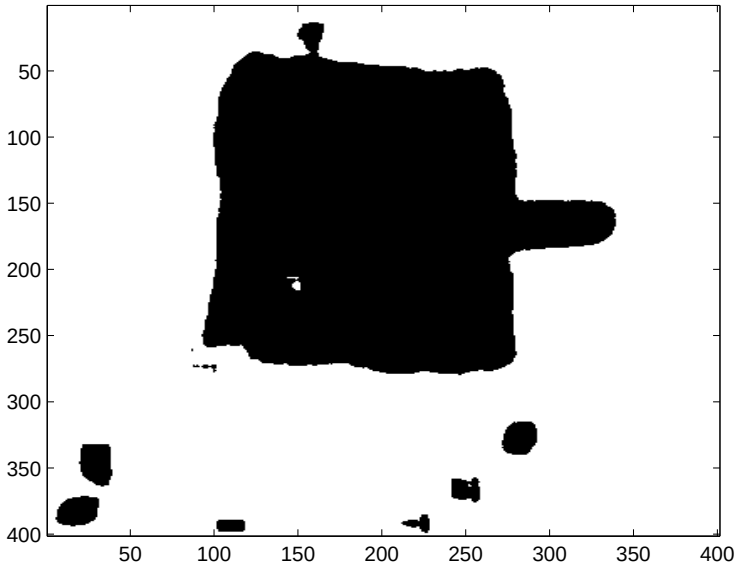

Figure A.26: Hybrid SVD_{25} change mask for Area F

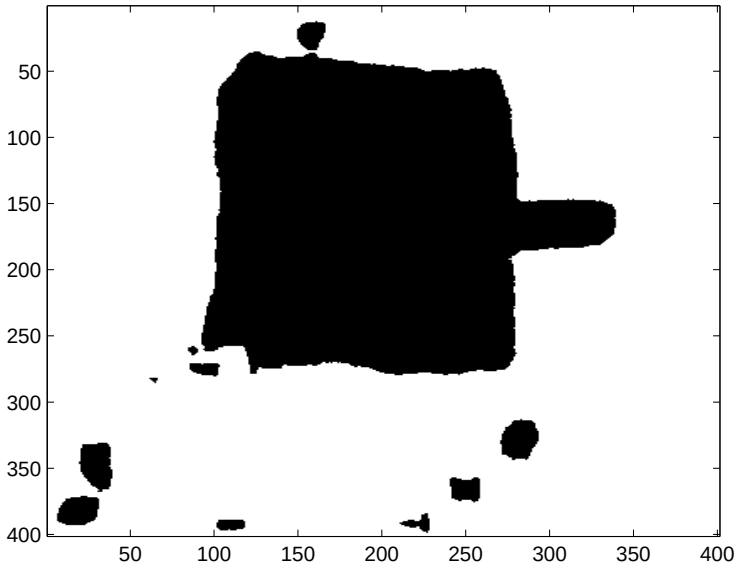

Figure A.27: Hybrid SVD_{50} change mask for Area F

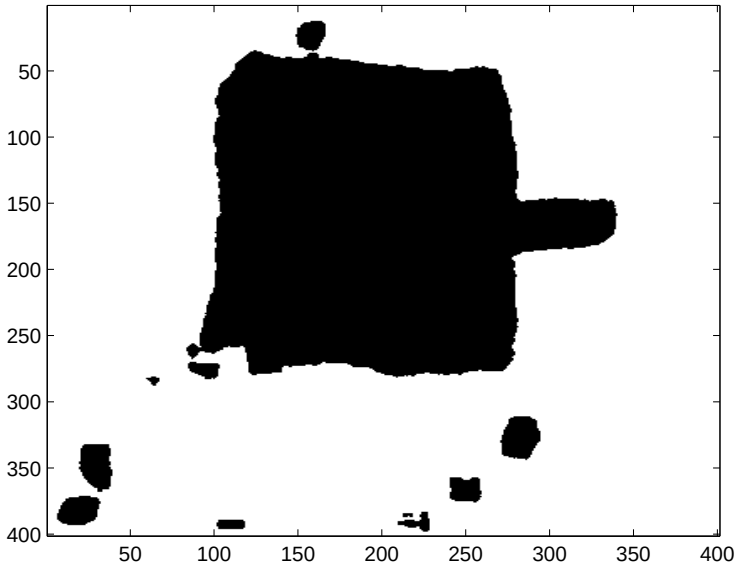

Figure A.28: Hybrid SVD_{75} change mask for Area F

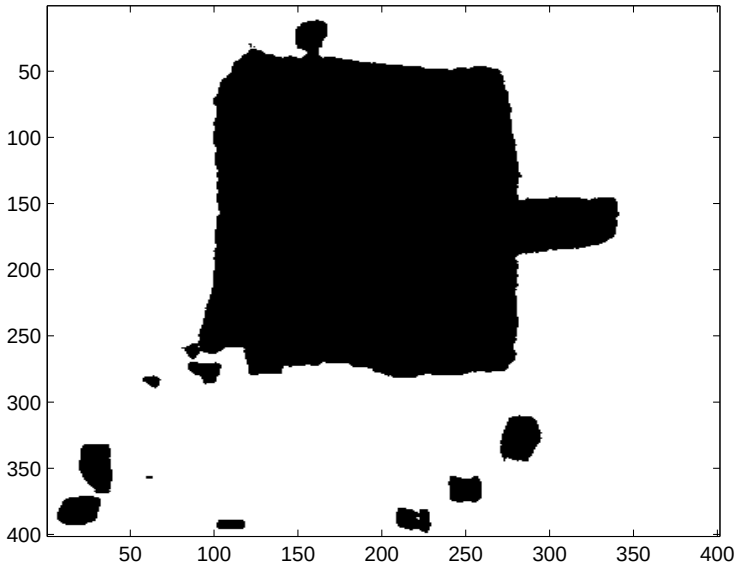

Figure A.29: Hybrid SVD_{100} change mask for Area F

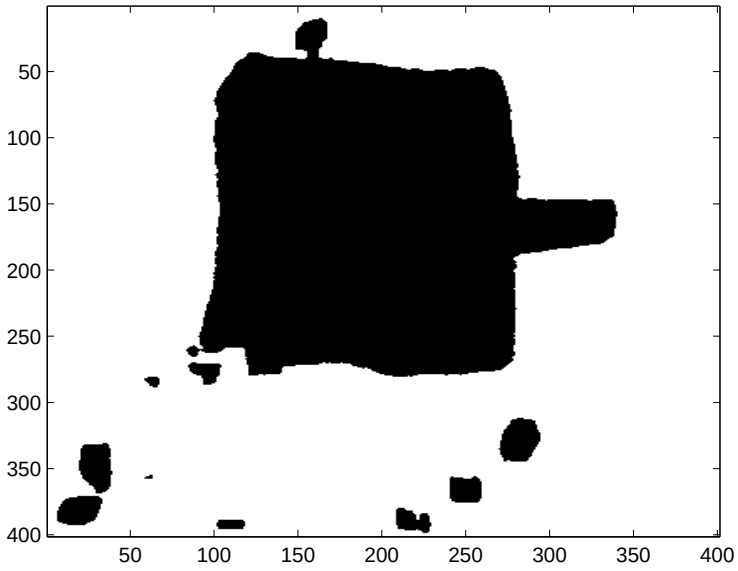

Figure A.30: Bi-orthogonal WT change mask for Area F with $\tau = 25$

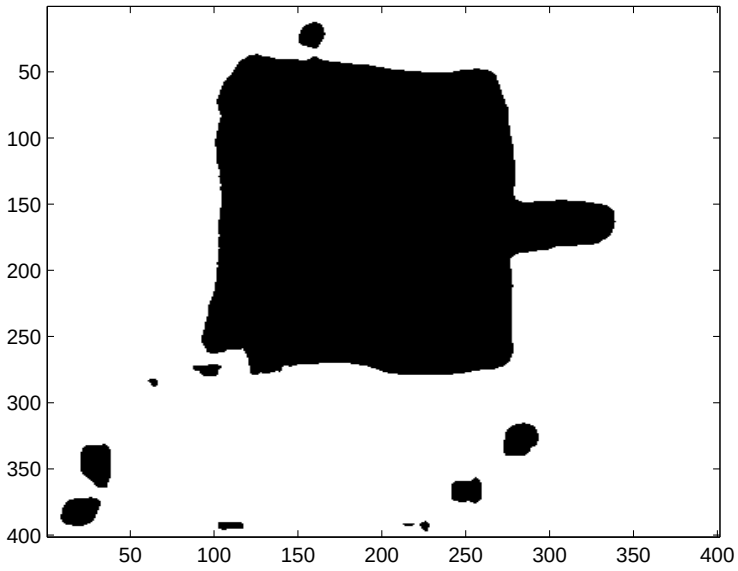

Figure A.31: Bi-orthogonal WT change mask for Area F with $\tau = 50$

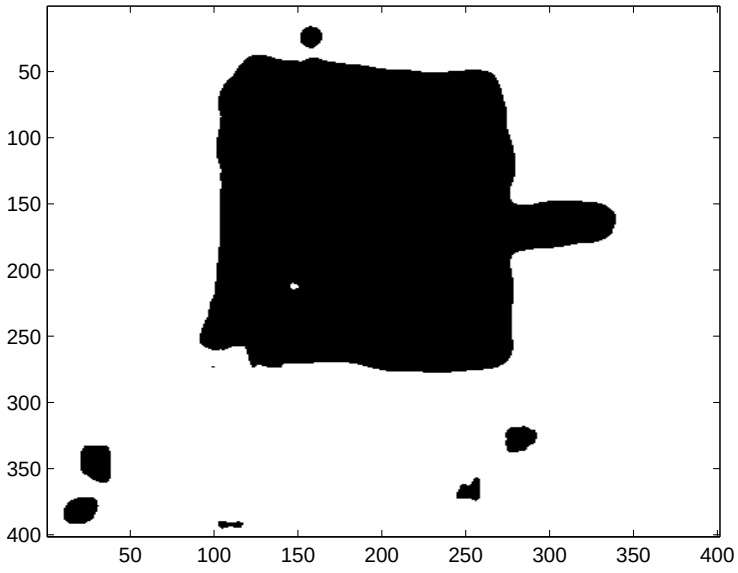

Figure A.32: Bi-orthogonal WT change mask for Area F with $\tau = 75$

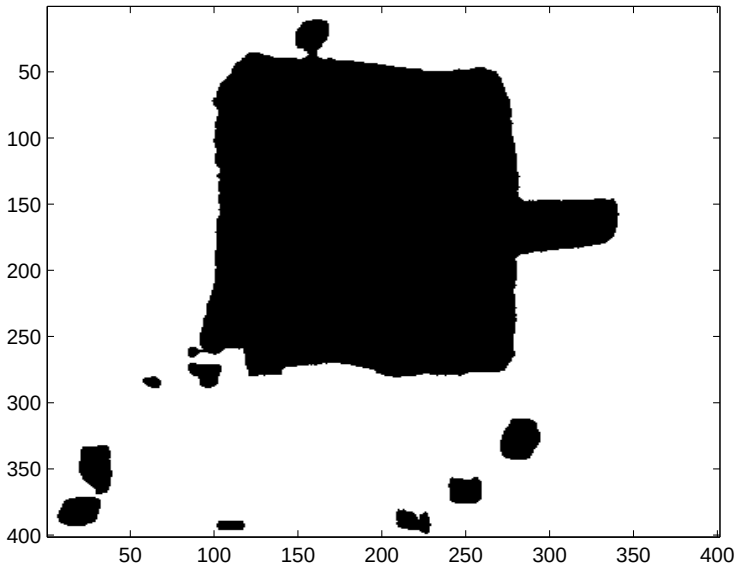

Figure A.33: Daubechies WT change mask for Area F with $\tau = 25$

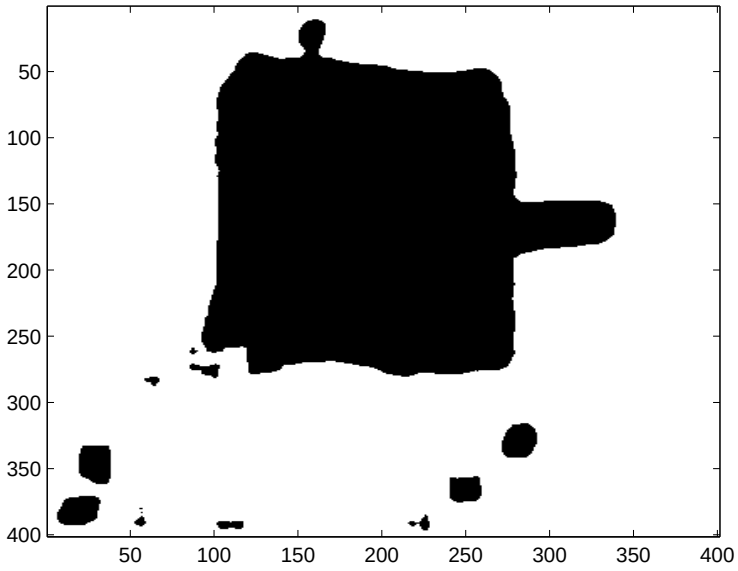

Figure A.34: Daubechies WT change mask for Area F with $\tau = 50$

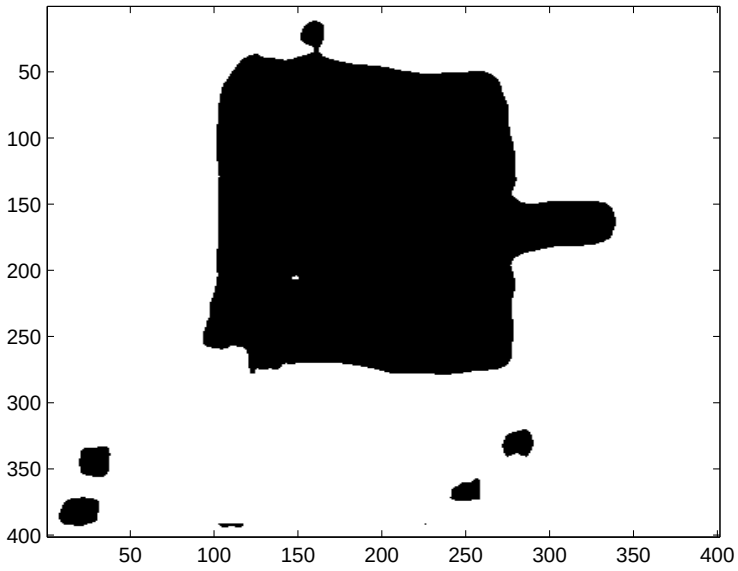

Figure A.35: Daubechies WT change mask for Area F with $\tau = 75$

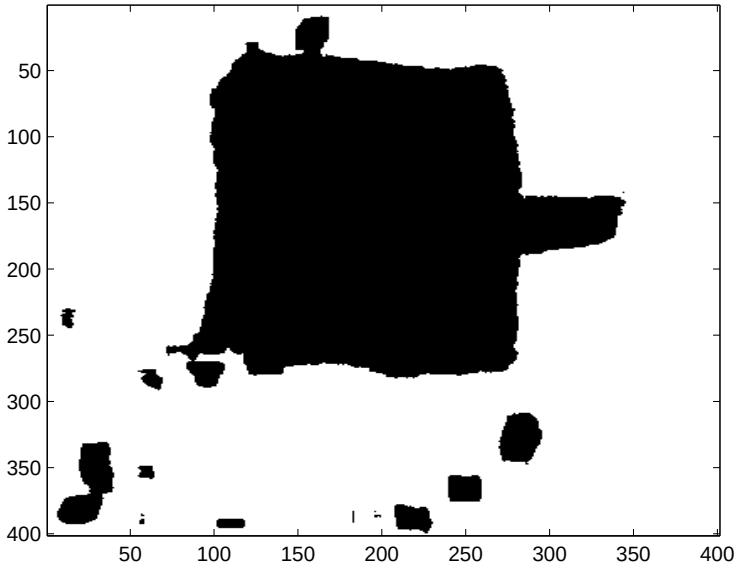

Figure A.36: JPEG based change mask

Bibliography

1. Aach, T. and A. Kaup. "Statistical model-based change detection in moving video". *Signal Process*, 31:165–180, 1993.

2. Ashino, Ryuichi, Akira Morimoto, Michihiro Nagase, and Remi Vaillancourt. *Image Compression using Multiresolution Singular Value Deomposition and other Methods*. In-House 14340045, Japanese Ministry of Education, Culture Sports, Science and Technology, Division of Information Sciences, Osaka Kyoiku Universitym Kashiwara, Osaka 582-8582, Japan, January 2004.

3. Cheney, Margaret. "Synthetic Aperture Radar". *SIAM News*, 35(4):14–15, 2002.

4. Dai, X. and S. Khorram. "The effects of image mis-registration on the accuracy of remotely sensed change detection". *IEEE Transactions on Geo-science and Remote Sensing*, 36(5):1566–1577, 1998.

5. Gupta, Savita and Lakhwinder Kaur. "Wavelet Based Image Compression using Daubechies Filters". URL `citeseer.ist.psu.edu/gupta02wavelet.html`.

6. Haykin, Simon. *Adaptive Filter Theory*. Prentice Hall, Upper Saddle River, NJ, fourth edition, 2002.

7. Ives, Robert W. "Lossless compression of waveform data using multiple-pass adaptive filtering". *Geoscience and Remote Sensing Symposium, 2000.*, volume 6, 2648–2650. Institute of Electrical and Electronics Engineers (IEEE), May 2000.

8. Kasetkasem, Teerasit and Pramod Kumar Varshney. "An Image Change Detection Algorithm Based on Markov Random Field Models". *IEEE Transactions on Geoscience and Remote Sensing*, 40(8):1815–1823, 2002.

9. Kou, Weidong. *Digital Image Compression Algorithms and Standards*. Kluwer Academic Publishers, Norwell, MA, 1995.

10. Legall, D. and A. Tabatabai. "Sub-band Coding of Digital Images using Symmetric Short Kernel Filters and Arithmetic Coding Techniques". *Acousitics, Speech and Signal Processing*, 11–14, 1988.

11. MacKay, David J. *Information Theory, Inference, and Learning Algorithms*. Cambridge University Press, Cambridge, United Kingdom, 2003.

12. Mathworks, The. "MATLAB r2007a".

13. Nikolaos V. Boulgouris, Athanasios Leontaris and Michael G. Strintzis. "Wavelet Compression of 3D Medical Images Using Conditional Arithmetic Coding". *IEEE International Symposium on Circuits and Systems*, 557–560. IEEE, IEEE, Thessaloniki, Greece, May 2000.

14. Novak, Leslie M. "Coherent Change Dection for Multi-Polarization SAR". *Signals, Systems and Computers, 2004. Conference Record of the Thirty-Ninth Asilomar Conference on*, 568–573. Institute of Electrical and Electronics Engineers (IEEE), IEEE Transactions on Signal Processing, Pacific Grove, CA, November 2005.

15. Oppenheim, Alan V., Ronald W. Schafer, and John R. Buck. *Discrete-Time Signal Processing*. Prentice Hall, Uppper Saddle River, NJ, second edition, 1999.

16. Poor, H. Vincent. *An Introduction to Signal Dection and Estimation*. Springer, Princeton, NJ, second edition, 1994.

17. Preiss, Mark and Nicholoas J. Stacy. *Coherent Change Detection: Theoretical Description and Experimental Results*. In-House DSTO-TR-1851, Defense Science and Technology Organization, Defense Science and Techology Organization, Edinburgh, South Australia, August 2006.

18. Radke, Richard J., Srinivas Andra, Omar Al-Kofahi, and Badrinath Roysam. "Image Change Detection Algorithms: A Systematic Survey". *IEEE Transactions on Image Processing*, 14(3):294–307, 2005.

19. Sameras, D. and D. Metaxas. "Incorporating Illumination Constraints in Deformable Models for Shape from Shading and Light Detection Estimation". *IEEE Transactions Pattern Analysis and Machine Intelligence*, 25(2):247–264, 2003.

20. See, Judi E. and Gilbert G. Kuperman. *Effects of SAR Image Compression on Image Interpretability and Detection Performance*. In-House AL/CF-TR-1996-0100, Air Force Research Laboratory, Air Force Research Labs, WPAFB, OH, June 1996.

21. Singh, A. "Digital change detection techniques using remotely-sensed data". *Int. J. Remote Sens.*, 10(6):989–1003, 1989.

22. Stearns, Samuel D. "Arithmetic Coding in Lossless Waveform Compression". *IEEE Transactions on Signal Processing*, 43(6):1874–1879, 1995.

23. Strang, Gilbert. *Linear Algebra and It's Applications*. Brooks Cole, Boston, MA, fourth edition, 2005.

24. Wallace, Gregory K. "JPEG Still Picture Compression Standard". *Communications of the ACM*, April 1991.

25. Wang, Hongqiang, S. Derin Babacan, and Khalid Sayood. "Lossless Hyperspectral Image Comrpession Using Context-based Conditional Averages". *2005 Data Compression Conference*, 1069–1075. IEEE, Chicago, Il, 2005.

26. Wang, Ye and Mikka Vilermo. "Energy Compaction Property of the MCDT in Comparison with Other Transforms". *109th Audio Engineering Society Convention, 2000 AES*, 1354–1362. AES, Audio Engineering Society, Tampere, Finland, September 2000.

27. Wang, Ze, Chi-Sing Leung, Yi-Sheng Zhu, and Tien-Tsin Wong. "Data compression on Illumination Adjustable Images by PCA and ICA". *Signal Processing: Image Communication*, 19(10):939–954, 2004.

28. Witzgall, Hanna E. and J. Scott Goldstein. *Signals, Systems and Computers, 2004. Conference Record of the Thirty-Eighth Asilomar Conference on*, 1675–1681. Institute of Electrical and Electronics Engineers (IEEE), Pacific Grove, CA, March.

29. Witzgall, Hanna E. and J. Scott Goldstein. "Exploiting Fundemental Properties of SAR Data for Compression of Tactical SAR Imagery". *Aerospace Conference, 2005 IEEE*, 1354–1362. Institute of Electrical and Electronics Engineers (IEEE), IEEE Aerospace and Electronic Systems Society, Big Sky, MT, November 2005.

30. Yuras, Gabriel. "Remote Sensing". Http://www.profc.udec.cl/ gabriel/tutoriales/rsnote/contents.htm.

REPORT DOCUMENTATION PAGE

Form Approved
OMB No. 0704–0188

1. REPORT DATE *(DD–MM–YYYY)*	2. REPORT TYPE	3. DATES COVERED *(From — To)*
13–09–2007	Master's Thesis	May 2006 — Sept 2007

4. TITLE AND SUBTITLE

THE EFFECTS OF SIGNAL AND IMAGE COMPRESSION OF SAR DATA ON CHANGE DETECTION ALGORITHMS

5a. CONTRACT NUMBER

5b. GRANT NUMBER

5c. PROGRAM ELEMENT NUMBER

6. AUTHOR(S)

Kiran Shenoy, 1st Lieutenant, USAF

5d. PROJECT NUMBER

5e. TASK NUMBER

5f. WORK UNIT NUMBER

7. PERFORMING ORGANIZATION NAME(S) AND ADDRESS(ES)

Air Force Institute of Technology
Graduate School of Engineering and Management
2950 Hobson Way
WPAFB OH 45433-7765

8. PERFORMING ORGANIZATION REPORT NUMBER

AFIT/GSS/ENG/07-02

9. SPONSORING / MONITORING AGENCY NAME(S) AND ADDRESS(ES)

Dr. Michael Minardi
AFRL-SNAS
2241 Avionics Circle
WPAFB, OH 45433
DSN:674-9269

10. SPONSOR/MONITOR'S ACRONYM(S)

11. SPONSOR/MONITOR'S REPORT NUMBER(S)

12. DISTRIBUTION / AVAILABILITY STATEMENT

Approved for public release; distribution is unlimited

13. SUPPLEMENTARY NOTES

14. ABSTRACT

With massive amounts of SAR imagery and data being collected, the need for effective compression techniques is growing. One of the most popular applications for remote sensing is change detection, which compares two geo-registered images for changes in the scene. While lossless compression is needed for signal compression, the same is not often required for image compression. In almost every case the compression ratios are much higher in lossy compression making them more appealing when bandwidth and storage becomes an issue. This research analyzes different types of compression techniques that are adapted for SAR imagery, and tests these techniques with three different change detection algorithms. Many algorithms exist that allow large compression ratios, however, the usefulness of the data is always the final concern. It is necessary to identify compression methods that will not degrade the performance of change detection analysis.

15. SUBJECT TERMS

synthetic aperture radar, compression, JPEG, wavelet transform, singular value decomposition, change detection

16. SECURITY CLASSIFICATION OF:			17. LIMITATION OF ABSTRACT	18. NUMBER OF PAGES	19a. NAME OF RESPONSIBLE PERSON
a. REPORT	b. ABSTRACT	c. THIS PAGE			Dr. Richard K. Martin
U	U	U	UU	110	19b. TELEPHONE NUMBER *(include area code)* rmartin@afit.edu, (937) 255–3636, ext 4625